Water Resources Research

RESEARCH ARTICLE
10.1029/2018WR024047

Key Points:
- The assumption of stationarity for meteorological drought risk estimation is evaluated in different parts of the CONUS at the multidecadal scale
- Nonstationarity is identified with statistical significance in the Northwest, upper Midwest, the Northeast, eastern Great Plains and in parts of Nevada, Utah, Arizona, and New Mexico in the Southwest United States
- Interdecadal changes in drought severity have not been statistically significant in California, Ohio valley, northern and western Great Plains, and the Southeast United States

Supporting Information:
- Supporting Information S1

Correspondence to:
X. Cai,
xmcai@illinois.edu

Citation:
Apurv, T., & Cai, X. (2019). Evaluation of the stationarity assumption for meteorological drought risk estimation at the multidecadal scale in contiguous United States. *Water Resources Research*, *55*. https://doi.org/10.1029/2018WR024047

Received 5 SEP 2018
Accepted 23 MAY 2019
Accepted article online 3 JUN 2019

Evaluation of the Stationarity Assumption for Meteorological Drought Risk Estimation at the Multidecadal Scale in Contiguous United States

Tushar Apurv[1] **and Ximing Cai**[1]

[1]Department of Civil and Environmental Engineering, University of Illinois at Urbana-Champaign, Urbana, IL, USA

Abstract In this study, we analyze the nonstationarity in meteorological droughts at the multidecadal scale in different parts of the contiguous United States during 1901–2017. We develop metrics to compare the drought risk calculated under the assumptions of stationarity and nonstationarity and identify their spatial and temporal patterns. By analyzing the variability of drought risk in the past and exploring its ongoing patterns, we evaluate in which regions of the contiguous United States the assumption of stationarity can be safely used for drought risk planning and management. We find statistically significant interdecadal changes in the probability distribution functions of drought severity in parts of the Northwest, upper Midwest, the Northeast, eastern parts of Great Plains and in parts of Arizona, New Mexico, Utah, and Nevada in the Southwest. In these regions, the nonstationary risk has been significantly higher than the stationary estimate of risk in the past, which shows that the assumption of stationarity can lead to the underestimation of drought risk in these regions. The multidecadal drought risk shows low variability in California, parts of northern and western Great Plains, Ohio Valley, and in the Southeast, since the statistical properties of droughts have not changed significantly in these regions during 1901–2017. However, the meteorological drought risk has increased in California and the Southeast in the recent decades due to the influence of global warming and hence the assumption of stationarity for risk estimation may lead to underestimation of drought risk in future in these regions if this effect of global warming persists.

Plain Language Summary Traditionally, statistical approaches adopted by water resource managers for planning and design of water resource systems and infrastructure are based on the assumption of stationarity; that is, it is assumed that the probabilistic characteristics of the hydrological and meteorological processes do not change with time, and hence, the planning and designs for future can be based on the past observations. In this paper, we have evaluated the validity of the stationarity assumption for meteorological drought risk estimation at the multidecadal scale by comparing drought risk calculated under the assumptions of stationarity and nonstationarity, respectively, in different parts of the continental United States. We find statistically significant nonstationarity in meteorological droughts in the Northwest, upper Midwest, the Northeast, eastern Great Plains and in parts of Nevada, Utah, Arizona, and New Mexico in the Southwest United States, which results in high interdecadal variability of drought risk in these regions. This result demonstrates that the assumption of stationarity can lead to underestimation of drought risk in these regions, thereby exposing water resource systems to failure under severe droughts.

1. Introduction

Droughts can last for multiple seasons or years and can hence cause widespread impacts on water resources, economy, environment, and society (World Meteorological Organization, 2006). In the United States, droughts rank among the costliest natural disasters. The droughts of 1930s and 1950s in the Great Plains and the Midwest droughts of 1988 and 2012 had a catastrophic effect on the agricultural productivity of the country. The 1988 drought resulted in economic losses of 40.8 billion $ (National Ocean and Atmospheric Administration, 2016), whereas the recent 2012 drought caused an economic loss of 30 billion $ (Rippey, 2015). The socioeconomic impacts of droughts are expected to further increase in the future due to the effects of increase in temperatures as well as the increasing human water demands, as it was evident in the recent California drought (Diffenbaugh et al., 2015; He et al., 2017). This has intensified the need for a

shift from emergency response-focused crisis management strategies to risk management strategies, which focus on drought impact mitigation through long-term planning (Cai et al., 2015; Wilhite et al., 2000).

Statistical approaches such as return periods, risk, and reliability are commonly used by water resource managers for planning and design of water resource systems and infrastructure, and hence constitute an essential component of risk management strategies. Traditionally, these approaches are based on the assumption of stationarity; that is, it is assumed that the probabilistic characteristics of the hydrological and meteorological processes do not change with time and hence the planning and designs for future can be based on the past observations. However, this assumption can be violated due to the changes in hydro-meteorological processes under the influence of climate change and anthropogenic activities (Milly et al., 2008, 2015). As a result, nonstationary statistical models have been proposed for the modeling of nonstationary processes, which account the variability of probability distribution parameters as a function of external covariates such as time or low-frequency climate signals (Katz et al., 2002). Numerous studies have applied these models for modeling the occurrences of extreme events such as extreme rainfall (Cheng & AghaKouchak, 2014; Steinschneider & Lall, 2015), floods (Lima et al., 2015; López & Francés, 2013; ; Sun et al., 2015; Towler et al., 2010), droughts (Du et al., 2015; Mondal & Mujumdar, 2015), snow water equivalent (Bracken et al., 2018), and extreme sea levels (Serafin & Ruggiero, 2014). Also, several new frameworks have been proposed for risk analysis under nonstationarity (Qi, 2017; Read & Vogel, 2015; Rootzen & Katz, 2013; Rosner et al., 2014; Salas & Obeysekera, 2014; Vogel et al., 2011; Volpi et al., 2015). While these studies have shown that the nonstationary models are able to improve the statistical representation of time series experiencing changes in statistical properties, the more complex structure of nonstationary models introduces additional uncertainty in the estimation of design events for planning and management (Serinaldi & Kilsby, 2015). This makes it important to ensure that the nonstationary models are used only if the nonstationarity in the time series is statistically significant. As a result, considerable research has been conducted for the development of statistical tests to detect gradual and abrupt changes in univariate (Rasmussen, 2001; Rouge et al., 2013; Wong et al., 2006; Xie et al., 2014; Yue et al., 2002) as well as multivariate (Chebana et al., 2013; Xiong et al., 2015) hydro-meteorological time series.

Most of the studies mentioned above have modeled and analyzed the nonstationarity of annual maximum rainfall and floods. Further, a number of these studies have analyzed the nonstationarity in annual maximum rainfall and floods at the regional, national, and even global scale (e.g., Archfield et al., 2016; Do et al., 2017; Ishak et al., 2013; Mallakpour & Villarini, 2015; Prosdocimi et al., 2015; Stahl et al., 2010; Villarini, Serinaldi, et al., 2009). While a number of studies have also analyzed the nonstationarity of droughts (Ahn & Palmer, 2016; Burke et al., 2010; Jiang et al., 2015; Kwon et al., 2016; Kwon & Lall, 2016; Mondal & Mujumdar, 2015; Osorio & Galiano, 2012; Sarhadi et al., 2016), none of the previous studies have analyzed the nonstationarity at the multidecadal time scale, which is the most relevant time scale for long-term planning and drought risk management (Wilhite et al., 2000). Also, most of the studies on the nonstationarity of droughts have been performed at the watershed or regional scale (e.g., Ahn & Palmer, 2016; Jiang et al., 2015; Mondal & Mujumdar, 2015; Sarhadi et al., 2016), and there are very few studies at the national scale (e.g., Burke et al., 2010). To our knowledge, no study has been published to analyze the nonstationarity of meteorological droughts at the national scale in the United States.

The analysis of nonstationarity in meteorological droughts at the multidecadal scale is particularly important in the United States, where the hydro-climatology and the hydro-climatic extremes are significantly influenced by multidecadal oscillations in the sea surface temperatures (SSTs) in the Atlantic and Pacific Oceans, namely, the Atlantic Multidecadal Oscillation (AMO) and the Pacific Decadal Oscillation (PDO; Enfield et al., 2001; Hoerling & Kumar, 2003; McCabe & Dettinger, 1999; Tootle et al., 2005). McCabe et al. (2004) have shown that changes in AMO and PDO have a significant influence on the meteorological drought risk in different parts of the United States at the decadal scale. This has further been verified by studies using climate models, which have shown that the changes in SSTs have been the dominant forcing of the major drought events in the twentieth century in the country, such as the droughts of 1930s and 1950s (Schubert et al., 2004a). Further, global warming has also influenced the long-term changes in precipitation in the United States in the twentieth century (Groisman et al., 2004). This motivates our study to analyze the multidecadal changes in meteorological droughts in the last century and to evaluate how safely the assumption of stationarity can be relied upon for the estimation of drought risk for planning and management of water resource systems in different parts of the country.

In this study, we analyze the nonstationarity in meteorological droughts at the multidecadal scale in different parts of the contiguous United States (CONUS) during 1901–2017. We use a moving window of multidecadal time scale to analyze how drought risk varies across decades at each grid point of a high-resolution precipitation data set for the CONUS. We define certain metrics to compare the multidecadal drought risk calculated using moving windows with the drought risk calculated assuming stationarity in the entire observation period. We also analyze the spatial patterns and temporal changes in these metrics to understand which regions of the CONUS have shown a relatively higher degree of variability of drought risk. By quantifying the variability of drought risk in the past and studying its ongoing changes, we evaluate how reasonable the assumption of stationarity is for drought risk estimation in different parts of the CONUS.

The rest of this paper is organized as follows. Section 2 provides the details of the methodology used in this study. Section 3 shows the results of the analysis in the form of spatial and temporal patterns of variability of drought risk. Section 4 discusses the results of the nonstationary analysis including the probable causes of the observed spatial and temporal patterns and the implications for drought risk management. Finally, section 5 concludes the paper with a summary of the results.

2. Materials and Methods

This section provides (i) data sets used in the study, (ii) methodology adopted for risk calculation, and (iii) definition of metrics for the quantification of variability of drought risk.

2.1. Data Set and Drought Definition

The focus of this study is on meteorological droughts, which are defined as deficits in precipitation. We use the Climate Research Unit monthly rainfall data set (CRU TS 4.02) that has a 0.5° spatial resolution and covers the period 1901 to 2017. Meteorological droughts are identified in this study using the Standardized Precipitation Index (McKee et al., 1993), which is recommended by the World Meteorological Organization for meteorological drought assessment. Here we use the Standardized Precipitation Index calculated at a six-month time scale (SPI6). We also performed the analysis using SPI3 to test the sensitivity of the results to the time scale of SPI, which is discussed later in the paper. A drought event is defined as the period when the value of SPI6 is below the threshold of −1 (moderate droughts). The length of a drought event is referred to as the duration of drought, whereas the severity of a drought event is defined as the cumulative deficit of SPI6 below the threshold during the event. In this study, we only focus on the severity of drought events.

2.2. Calculation of Drought Risk

First, we define certain terms involved in risk-based design of water resource systems. A design drought event is defined as the drought event for which a water resource system or structure is designed; that is, the system or the structure can successfully operate until the design event is exceeded (Joseph, 1970). The project life is defined as the duration of time for which the system or structure is designed. The risk of the design event during the project life is the probability that the design event will be exceeded at least once during the project life (Chow, 1964).

In this study, stochastic simulation of drought events is used for drought risk estimation, using the methodology suggested by Salas et al. (2005). According to this method, to find the risk associated with a drought event of severity S_o during a project life of n years, a time series model needs to be developed to replicate the statistical properties of the observed time series. If the risk is to be estimated for a project life of n years, the time series model is used to simulate a large number (N) of synthetic time series sequences of length n years. Then the number of simulations out of N, in which the design event severity S_o is exceeded at least once, is counted. Denote this number as e. Then the risk of design event S_o in the project life of n years is given by

$$\text{Risk} = \frac{e}{N} \tag{1}$$

For each grid point in the observation data set, we calculate the risk associated with a design event (S_o) assuming stationarity and nonstationarity and compare the values of the two estimates.

2.2.1. Annual Precipitation T Series Modeling

As mentioned above, a time series model is needed, which can be used for the stochastic simulation of droughts and then for risk calculation. Traditionally, linear parametric models such as Autoregressive

Moving Average have been most commonly used for time series modeling, but they rely on assumptions such as normal distribution of variables and a linear dependence between successive time steps, which can be violated in hydrologic time series (Box & Jenkins, 1976; Bras & Rodriguez-Iturbe, 1985). Nonparametric methods, such as k-nearest neighbor (KNN) bootstrap resampling, overcome these drawbacks of linear parametric models, but are unable to simulate values outside the range of the historical data (Mehrotra & Sharma, 2007; Rajagopalan & Lall, 1999; Sharma et al., 1997; Srinivas & Srinivasan, 2005). A detailed overview of these models can be found in Rajagopalan et al. (2010). Generalized linear models (GLMs) (Coe & Stern, 1982) offer an alternative to these approaches, and are able to model nonnormal and nonlinear time series by modeling the parameters of probability distribution functions of variables as a function of external covariates through link functions. The main advantage offered by GLMs is that it explicitly allows variables to be linked with external covariates such as low-frequency climate signals, thereby enabling the model to capture the low-frequency variability in the observed time series. The ability of time series models to capture low-frequency variability is crucial for multidecadal drought risk estimation, since the low-frequency variability in precipitation time series has a significant impact on the changes in the drought risk at the multidecadal scale. That is why, in this study, we use the generalized additive model for location, scale, and shape (GAMLSS; Rigby & Stasinopoulos, 2005), which is a variant of GLM, for simulating the precipitation time series in this study. The advantage of GAMLSS over GLM is that GLM requires the observations of the time series to have the exponential family of distributions as the underlying distribution. However, there is no such restriction in GAMLSS, allowing time series modeling for observations with any underlying distribution (Rigby & Stasinopoulos, 2005). Because of its ability to relate time series variables with external covariates, GAMLSS has been employed by many studies for nonstationary modeling and attribution (Jiang et al., 2015; López & Francés, 2013; Tan & Gan, 2015; Villarini, Smith, et al., 2009; Villarini et al., 2010, 2011; Xiong et al., 2018; Zhang et al., 2014, 2015). GAMLSS has also been used for stochastic simulation of climate variables and in weather generators (Chun et al., 2013; Serinaldi & Kilsby, 2012, 2014; Tye et al., 2016; Verdin et al., 2015). For example, Serinaldi and Kilsby (2012) used GAMLSS for stochastic modeling of monthly precipitation at multiple sites in the United Kingdom. They demonstrated that the model could not only capture the statistical properties of monthly precipitation but was also successful in reproducing the drought properties such as duration and severity, making it a useful tool for drought risk assessment.

We use GAMLSS for simulating the annual precipitation time series, which is then disaggregated to monthly time series. We adopt this approach because previous studies have shown that daily and monthly weather generators produce simulations that tend to be overdispersed at the annual time scale and are unable to reproduce the low-frequency persistence of observed time series (e.g., Katz & Parlange, 1998; Wilks, 1999). To overcome this problem, several studies have proposed modeling the low-frequency component explicitly and then superimposing the high-frequency components of the time series (e.g., Kwon et al., 2007; Steinschneider & Brown, 2013). Following these studies, we have used GAMLSS for explicitly modeling the low-frequency component in the annual precipitation time series and then disaggregated the annual values into monthly values.

The model structure of GAMLSS, described in Rigby and Stasinopoulos (2005), is briefly introduced as follows. If Y is the variable whose time series is to be simulated using GAMLSS, it is assumed that the independent observations of Y denoted by y_i (i = 1,2, ... n) have a cumulative probability distribution function $F_Y(y_i, \theta^i)$ with $\theta^i = \left(\theta^i_1, \theta^i_2 ..... \theta^i_p\right)$ being a vector of p distribution parameters accounting for location, scale, and shape. Commonly p is less than or equal to 4, depending on the type of the distribution selected, as one-, two-, three-, and four-parameter distributions provide sufficient flexibility for most applications. For a given "n" length vector of the response variable $\boldsymbol{y} = (y_1, y_2 \ldots \ldots . y_n)^T$, $g_k(.)$ for $k = 1, 2 \ldots p$ are defined as link functions relating the distribution parameters to explanatory variables and random effects through an additive model given by

$$g_k(\theta_k) = \eta_k = \boldsymbol{X_k}\boldsymbol{\beta_k} + \sum_{j=1}^{J_k} \boldsymbol{Z_{jk}}\boldsymbol{\gamma_{jk}} \tag{2}$$

where θ_k and η_k are vectors of length n. $\theta_k = \left(\theta^1_k, \theta^2_k, ...\theta^n_k\right)^T$ represents the values of the kth parameter of the distribution function at time steps 1,2 ... n and η_k is the vector containing the corresponding values of the

link function. J_k is the number of explanatory variables and $\boldsymbol{X_k}$ is a $n \times J_k$ matrix containing the values of these predictors at the n time steps. $\boldsymbol{\beta_k} = \left(\beta_{1\,k}, \beta_{2\,k}, \ldots\ldots \beta_{J_k k}\right)^T$ is the parameter vector, which needs to be determined. $\boldsymbol{Z_{jk}}$ is a fixed known design matrix of dimension $n \times q_{jk}$ and $\boldsymbol{\gamma_{jk}}$ is a q_{jk} dimensional random variable.

Equation (2) can be used to obtain the relation between all the parameters $k = 1,2 \ldots . p$ of the distribution function F_Y with the selected explanatory variables. The linear prediction function is composed of two components: parametric component $\boldsymbol{X_k \beta_k}$ (linear function of explanatory variables) and random component $\boldsymbol{Z_{jk} \gamma_{jk}}$. Parameters $\boldsymbol{\beta_k}$ in equation (2) are estimated using the maximum likelihood principle. The best model can be selected using Akaike information criteria (Akaike, 1974). The details about the model fitting and selection can be found in Rigby and Stasinopoulos (2005). Once the GAMLSS model is trained and selected, the time series can be generated by the simulation of standard uniform random numbers. The random numbers can be used to generate the time series by applying the probability integral transform to the time-varying probability distribution functions. One of the requirements of the GAMLSS model is that the observations of the variable being simulated (Y) need to be independent of each other. However, previous studies have shown that GAMLSS is able to reproduce the statistical properties of the observed time series even when this condition is not strictly fulfilled (Serinaldi, 2011; Villarini & Serinaldi, 2012).

In this study, we use GAMLSS to simulate the annual precipitation time series at each grid point in the observation data set (i.e., response variable y represents annual precipitation). We consider three probability distribution functions: gamma, lognormal, and Weibull distributions as candidates for modeling annual precipitation, based on the findings of previous studies which have performed distribution fitting for annual precipitation in the CONUS (Guttman et al., 1993; Markovic, 1965). The best distribution at each site was selected as the one with the lowest Akaike information criterion value (Figure S1). Time is used as the explanatory variable in our study and the parameters of the probability distributions are modeled as a fifth-order polynomial function of time, so that there is sufficient flexibility to capture the decadal changes in annual precipitation. The logarithmic function is chosen as the link function. Thus, in equation (2) at any time t,

$$g\left(\theta_k^t\right) = \log\left(\theta_k^t\right) \tag{3}$$

$$X_k^t\, \boldsymbol{\beta_k} = \beta_0 + \beta_1 t + \beta_2 t^2 + \beta_3 t^3 + \beta_4 t^4 + \beta_5 t^5 \tag{4}$$

where θ_k^t is the value of the parameter θ_k at time t; X_k^t is the t^{th} row of the matrix $\boldsymbol{X_k}$; t = 1901, 1902 ... , 2017; and $k = 1, 2$ since the distributions are two-parameter distributions. Thus, in our study the length of the time series at each grid point is T = 117 years. We perform the GAMLSS simulation using the GAMLSS package (Stasinopoulos & Rigby, 2007) in the software R.

2.2.2. Disaggregation of Annual Precipitation

The annual precipitation time series generated using GAMLSS needs to be disaggregated to monthly time series so that monthly SPI values can be calculated for estimating drought risk. Numerous techniques have been employed in literature for the disaggregation of annual precipitation and streamflow time series. Linear stochastic disaggregation techniques disaggregate annual time series linearly into monthly values by assuming that both the annual and monthly variables are normally distributed, and hence require the data to be transformed to normal distribution prior to disaggregation (Mejia & Rousselle, 1976; Santos & Salas, 1992; Stedinger & Vogel, 1984; Valencia & Schakke, 1973). However, the back transformation of the disaggregated values in the original space does not guarantee that the monthly values will add up to the annual values. These techniques have been modified by some studies to avoid the need for transformation, but they still rely on the assumption of linearity (Koutsoyiannis, 1999, 2001). An alternate to these models is a nonparametric model, in which the disaggregation function is fitted locally to a limited number of neighbors at each point rather than fitting functions to the entire data set (Kumar et al., 2000; Sharma et al., 1997; Tarboton et al., 1998). This allows the nonparametric models to capture the nonnormal and nonlinear characteristics of the time series. In this study, we apply one such nonparametric approach developed by Prairie et al. (2007), which is based on the KNN algorithm. This approach has been applied successfully by many other studies for the disaggregation of streamflow and precipitation time series (e.g., Bracken et al., 2010; Kalra & Ahmad, 2011; Lu et al., 2016; Sinha et al., 2014; Wang et al., 2015). A brief description of this approach is provided in Appendix A.

2.2.3. Nonstationary Drought Risk

In this study, we use a moving window approach to understand how the drought risk has changed at the multidecadal scale. We choose a design event with drought severity S0 and calculate the drought risk associated with the design event in each moving window based on the statistical properties of droughts during that window. The length of the moving window needs to be chosen such that the window is long enough to characterize the statistical properties of droughts during that period, but at the same time, the time series can be assumed stationary within the moving window. Guttman (1989) suggested that a duration of 30 years can be used to characterize the climate of a given place. Kao and Ganguly (2011) recommended the use of a 30-year window for studying the influence of multidecadal oscillations. A number of other studies have also used 30-year windows for nonstationary analysis of time series (Ghosh et al., 2012; Gilroy & McCuen, 2012; Jain & Lall, 2001; Qi, 2017; She et al., 2015; Vittal et al., 2013). Following these studies, we also use a 30-year moving window in this study. By using a 30-year moving window, we assume that the statistical properties of climate remain stationary within each 30-year period. Hence, for calculating the drought risk, we assume that the project life n is the same as the length of the moving window, that is, $n = 30$, to ensure that the project life, for which the risk is being calculated, is not longer than the period of assumed stationarity in drought properties. If we denote a moving window by its last year, the t^{th} moving window $mw(t)$ will consist of data points $[y_{t-29}, y_{t-28}, \ldots \ldots . y_t]$, where y_t is the annual precipitation in year t. Since we have 117 years of data for each grid point, there will be 88 such moving windows with $t \in \{1930,1931 \ldots \ldots \ldots 2017\}$. While calculating drought risk using the nonstationary approach, we assume that the statistical properties of droughts are different for each moving window. However, it should be noted that the risk calculated for successive moving windows will be correlated due to the overlapping of moving windows. In order to calculate the drought risk in the t^{th} moving window, the stochastic simulation of drought events should be based on the statistical properties of the observed precipitation time series during the 30 years of the t^{th} moving window. Therefore, for calculating the nonstationary drought risk in moving window $mw(t)$, we first use the time series model to replicate the statistical properties of the observed precipitation time series during the 30 years of the moving window (i.e., $t \in \{t-29, t-28 \ldots \ldots \ldots, t\}$) and then use it for drought risk calculation. The steps for calculating the nonstationary drought risk for the design event S_0 in $mw(t)$ are as follows:

1. First, generate a large number ($N = 1{,}000$) of synthetic 30-year samples of annual precipitation $[y_{t-29}, y_{t-28}, \ldots \ldots . y_t]$ by substituting $[t-29, t-28, \ldots \ldots \ldots . t]$ into the GAMLSS model (equation (4)). This step produces multiple annual precipitation time series sequences, which follow the statistical properties of the observed time series during the period of the moving window.
2. Next, disaggregate each of the N time series sequences generated in step 1 using the KNN disaggregation algorithm described in section 2.2.2. Use the disaggregated time series to calculate the severity of drought events.
3. Finally, count the number of time series samples, in which the design event severity S_0 is exceeded at least once. Let this number be denoted by $e(t)$. The drought risk for the event of severity S_0 in $mw(t)$ is then calculated as

$$Risk_{ns}(t) = \frac{e(t)}{N} \tag{5}$$

where $Risk_{ns}(t)$ denotes the nonstationary risk in the t^{th} moving window. In steps 1 and 2, we use the time series model for the stochastic simulation of drought events based on the statistical properties of the observed precipitation time series during the 30 years of the t^{th} moving window $t \in \{t-29, t-28 \ldots \ldots \ldots, t\}$, which we then use for calculating the drought risk in step 3.

2.2.4. Stationary Drought Risk

While calculating the nonstationary drought risk, we assume that the statistical properties of droughts are different in each moving window. However, under the assumption of stationarity, the statistical properties of droughts are assumed to be the same during the entire observation period, and hence, all the observed drought events in the past are considered for risk calculation. Thus, instead of sampling multiple time series sequences from a fixed 30-year period, we now sample 30-year sequences randomly from the entire observation period. The steps for the calculation of stationary drought risk are as follows:

1. First, randomly sample N values of t with repetition, such that $t \in \{1930,1931 \ldots \ldots \ldots 2017\}$. For each value of t, generate a 30-year sample of annual precipitation $[y_{t-29}, y_{t-28}, \ldots \ldots . y_t]$ by substituting

$[t-29, t-28, \ldots \ldots \ldots . t]$ into the GAMLSS model (equation (4)). This step is performed to randomly sample a 30-year time series sequence from the entire record so that all drought events observed in the past are considered in risk calculation.

2. Disaggregate each of the N time series sequences generated in step 1 using the KNN disaggregation algorithm and use the disaggregated time series to calculate the severity of drought events.
3. Count the number of time series samples, in which the design event severity S_0 is exceeded at least once. Denoting this number by "e," the stationary drought risk for the event of severity S_0 is given by

$$Risk_s = \frac{e}{N} \tag{6}$$

where $Risk_s$ denotes the risk calculated assuming stationarity.

The main difference between the risk calculation using the nonstationary approach (equation 5) and the stationary approach (equation (6)) is further explained as follows: with the nonstationary approach, we calculate the drought risk during a given 30-year period based on the statistical properties of droughts in that period only. However, with the stationary approach, we calculate the drought risk based on the assumption that all drought events observed in the past (117 years considered in this study) have the same statistical properties. That is to say, all the drought events occurring in the study period are used for the calculation of drought risk in the stationary approach, and a single estimate of risk is obtained for the entire study period, which remains unchanged across the entire observation period, as opposed to a time series of risk obtained from each of the 30-year time window by the nonstationary approach.

While we have adopted a numerical approach in this study, an analytical approach for calculating drought risk has also been proposed by a previous study (Loaiciga, 2005), which involves distribution fitting via parameter estimation. With the nonstationary approach, we need to compute the drought risk separately for each 30-year period. However, there may not be a sufficiently large number of drought events during a 30-year window for reliable estimation of the distribution parameters. While with the numerical approach, a large number of synthetic time series sequences are generated first. This procedure provides sufficient samples of drought events, which allows a more reliable calculation of the drought risk. Thus, we adopt the numerical approach to estimate the nonstationary meteorological drought risk in this study.

According to the definition of risk, it is the probability that the design event is exceeded at least once in the planning period. Since our objective is to analyze the temporal changes in drought risk, we should select a design event that does not have a very low or a very high probability of exceedance in the 30-year period. For example, if we choose the 100-year return period event as the design event, the probability of exceedance of such an extreme event can be zero or very close to zero in many of the moving windows, which can make it difficult to understand the temporal patterns of changes in drought risk. That is why, in this study, we choose the value of S_o to be the drought severity with a return period of 30 years, which is expected to occur once in every 30 years on an average in the long run. We calculate the magnitude of design event S_o using the relationship between drought severity and its return period, given by Shiau and Shen (2001):

$$T_s = \frac{E(L)}{1-F_S(S_0)} \tag{7}$$

where T_s is the return period (set equal to 30 years), $E(L)$ is the average interarrival time between any two successive drought events, and F_S denotes the cumulative distribution function of drought severity. We use equation (7) to determine the design event for each grid point and then use equations (5) and (6) to calculate the risk associated with this event under the assumptions of nonstationarity and stationarity, respectively.

2.3. Quantification of Drought Risk Variability

Next, we define certain metrics for the quantification and comparison of the variability of drought risk in different parts of the CONUS. Due to the multidecadal oscillations in climate, the nonstationary risk at any point of time can be higher or lower than the stationary risk. From a planning and management perspective, the periods in which the nonstationary risk is higher than the stationary risk need more attention, since the underestimation of risk in these periods can lead to the failure of water resource systems and

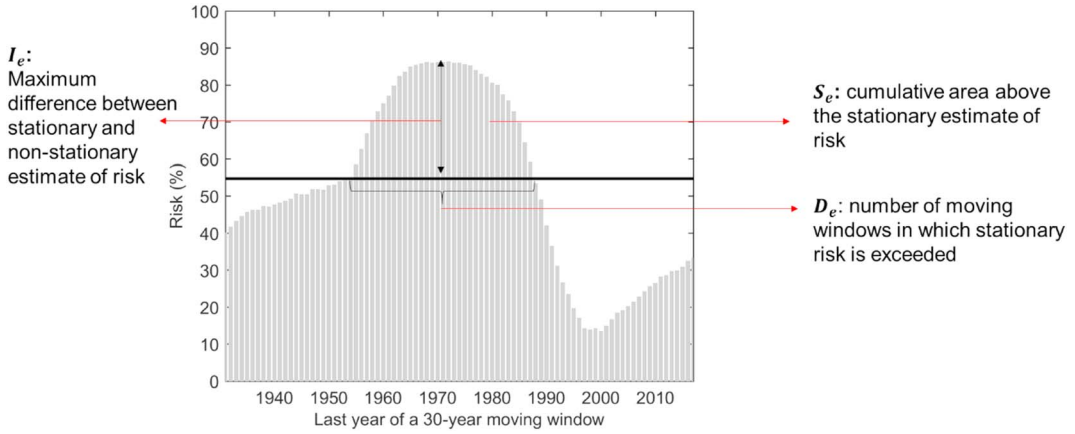

Figure 1. Definition of metrics used to quantify the variability of drought risk. The grey bars represent the nonstationary risk calculated using moving windows and the black line represents the stationary risk. The *x* axis shows the *last year* of a moving window.

infrastructure. Thus, in this study, we focus on those periods and we call these periods as stationary risk-exceedance periods, denoted by $t_e = \{t \mid Risk_{ns}(t) > Risk_s\}$.

We further define the following metrics to characterize the stationary risk-exceedance periods:

1. Risk exceedance duration D_e: The number of moving windows (out of 88) in which the nonstationary risk is higher than the stationary drought risk.
2. Risk exceedance severity S_e: The cumulative surplus of nonstationary risk over the stationary risk calculated across all risk-exceedance periods:

$$S_e = \sum_{t \in t_e} (Risk_{ns}(t) - Risk_s) \tag{8}$$

3. Risk exceedance intensity I_e: The maximum difference between the nonstationary and stationary risk over all the risk-exceedance periods:

$$I_e = \max(Risk_{ns}(t) - Risk_s), \quad t \in t_e \tag{9}$$

These metrics are illustrated in Figure 1 below. In the figure, the grey bars represent the nonstationary risk calculated using moving windows and the black solid line shows the stationary risk calculated for a grid point in the observation data set.

3. Results

3.1. Validation of Time Series Model

First, we evaluate the capability of the time series model to reproduce the statistics of the observed time series. We compare the value of a particular statistic of the observed time series with the median value of the statistic from 1,000 simulations generated by the time series model at each grid point. The details of model validation are provided in the supporting information. Figure S2 shows the comparison of the statistics of the observed and modeled annual precipitation time series, whereas Figures S3–S6 show the comparison for the monthly statistics. For both monthly and annual scales, four statistics are compared: mean, standard deviation, skewness, and lag-1 autocorrelation. For most of the locations in the observation data set, the observed statistics at the annual scale lie within the range of the statistics of the time series generated by the GAMLSS model. Also, the statistical metrics of the monthly time series, generated by the disaggregation of the annual time series, match well with those of the observed time series. These results show that the GAMLSS model, combined with the KNN-based disaggregation, is able to reproduce the statistics of the observed time series at both the annual and monthly time scales. In Figure S7, we also compare the observed and modeled severities of drought events at four different levels: 25th, 50th, 75th, and 95th percentiles (Q25,

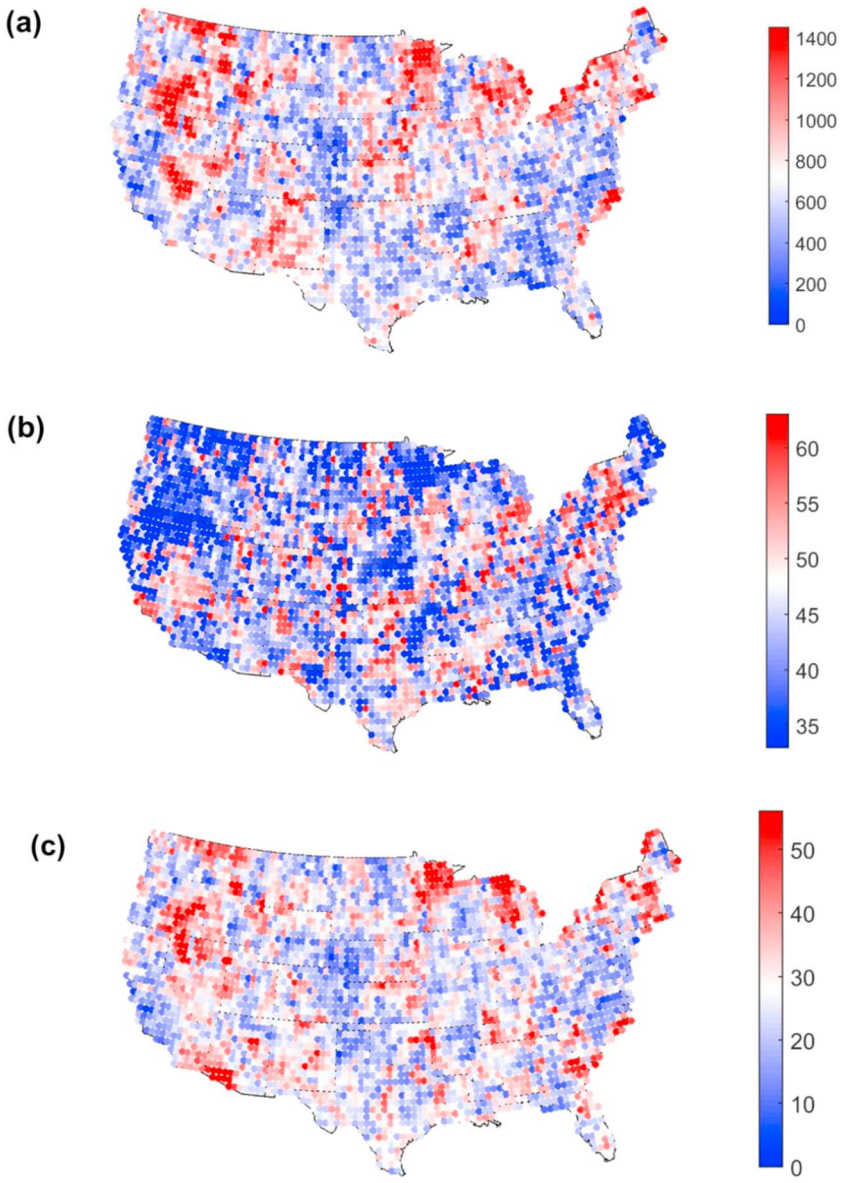

Figure 2. Spatial distribution of (a) S_e, (b) D_e,and (c) I_e (D_e represents the number of moving windows in which the nonstationary risk is higher than the stationary risk and the total number of moving windows is 88).

Q50, Q75, and Q95, respectively) drought severity during 1901–2017. For most of the locations in the CONUS, the observed drought severities at all the four levels lie within the modeled range, showing that the time series model is capable of modeling both the low- and high-severity drought events that have occurred in the past.

3.2. Spatial Patterns of Drought Risk Variability

The spatial distribution of the metrics S_e, D_e, and I_e are shown in Figure 2. The color scheme used in the figure implies that the nonstationary risk has exceeded the stationary risk to a greater extent at the red colored points relative to the blue colored points. From Figure 2, it can be seen that the risk exceedance severity S_e and intensity I_e are highly correlated as their spatial patterns are very similar (Figures 2a and 2c). There are clusters of grid points with high values of S_e in the following regions: (1) Oregon and Washington in the Northwest; (2) Nevada, Utah, Arizona, and New Mexico in the Southwest; (3) Tennessee, Nebraska, and Kansas in Central United States; (4) Minnesota and Michigan in the upper

Midwest; and (5) in most of Northeast United States. This shows that these five regions have experienced larger exceedance of stationary drought risk due to higher interdecadal variability of drought risk in the past. On the other hand, there has been a smaller exceedance of the stationary drought risk due to low interdecadal variability of drought risk in (1) California along the west coast; (2) North Carolina, South Carolina, Georgia, and Alabama in the Southeast; (3) parts of northern and western Great Plains including Wyoming, eastern Colorado, and western Nebraska; and in (4) the Ohio valley in the Midwest. The risk exceedance duration D_e shows a different pattern as compared to those of S_e and I_e. The Northwest U.S. and the upper Midwest regions show high values of S_e and I_e but low values of D_e. This implies that in these regions, the exceedance of the stationary risk was high but for a short duration of time. On the other hand, in the northern and central parts of Texas, the magnitude of risk exceedance is small, but the stationary risk has been exceeded for a long duration.

3.3. Temporal Patterns of Drought Risk Variability

In Figure 3, we show the changes in the 95th percentile drought severity (Q95) calculated using the 30-year moving windows for nine locations selected from across the CONUS. These locations have been selected because they represent the characteristics of the changes in the drought severity in the regions from where they have been selected. These include five locations from the regions with high multidecadal variability and four from the regions with low multidecadal variability of drought risk. Figure 3 also shows the Q95 drought severity in different moving windows generated in the 1,000 simulations of the time series models. The dark grey bars show the interquartile range and the light grey bars show the complete range of the simulated values at each of these locations. As it can be seen in the figure, the black lines representing the observed values lie within the simulated range in all the moving windows. This shows that the time series model is able to capture the multidecadal changes in the magnitude of extreme drought events. How the nonstationary risk has changed in these locations is shown in Figures 4–6.

Figure 4 shows the changes in drought risk for four locations in Oregon, Minnesota, Kansas, and Tennessee. The grey bars show the nonstationary risk calculated using equation (5) and the black solid line shows the stationary risk calculated using equation (6). At all these four locations, the nonstationary drought risk is very high compared to the stationary drought risk in the early part of the twentieth century. The nonstationary risk peaks during the 1911–1940 moving window and declines in the following windows. The high risk during this period was a result of the Dust Bowl droughts of 1930s, which affected parts of the Northwest United States, northern and central Great Plains, and parts of the Midwest (Cook et al., 2014).

Figure 5 shows the changes in drought risk for another set of five locations selected from Nevada, New Mexico, Texas, Massachusetts, and Arizona. In these five regions, the nonstationary drought risk is high during the midtwentieth century. The nonstationary drought risk peaks during the 1941–1970 moving window for Nevada, New Mexico, Texas, and Arizona, whereas it peaks slightly later in the 1951–1980 moving window in Massachusetts. The high drought risk in Nevada, New Mexico, Arizona, and Texas during the 1941–1970 moving window is a result of the 1950s droughts, which had the most significant impact in the southwest and southern Great Plains (Hoerling et al., 2009). The Northeast United States also experienced a severe drought in the 1960s, which is indicated by the significantly increased drought risk level during the 1951–1980 period (Namias, 1966).

By looking back at Figure 2, we can see that the regions affected by the Dust Bowl and the 1950s drought show similar severity of risk exceedance (S_e), but the duration of risk exceedance (D_e) is much smaller for the regions affected by the Dust Bowl droughts. As a result, the regions affected by the Dust Bowl droughts have a higher risk exceedance intensity (Figure 2c). For example, Oregon (Figure 4a) and Nevada (Figure 5a) have a similar magnitude of S_e, but the nonstationary risk is higher than the stationary risk in Oregon only for roughly 30 moving windows as opposed to around 40 windows in Nevada. This is because the Dust Bowl droughts of 1930s were followed by an abrupt transition from dry to wet conditions in the 1940s, which affects the estimate of drought risk (rapid reduction) in the following years (Schubert et al., 2004b).

The nonstationary and stationary drought risk for the remaining four locations selected from California, North Carolina, Wyoming, and Ohio are shown in Figure 6. The S_e values in these four regions are among the lowest in the CONUS. As is evident from the figure, the reason for the low S_e values in these regions is

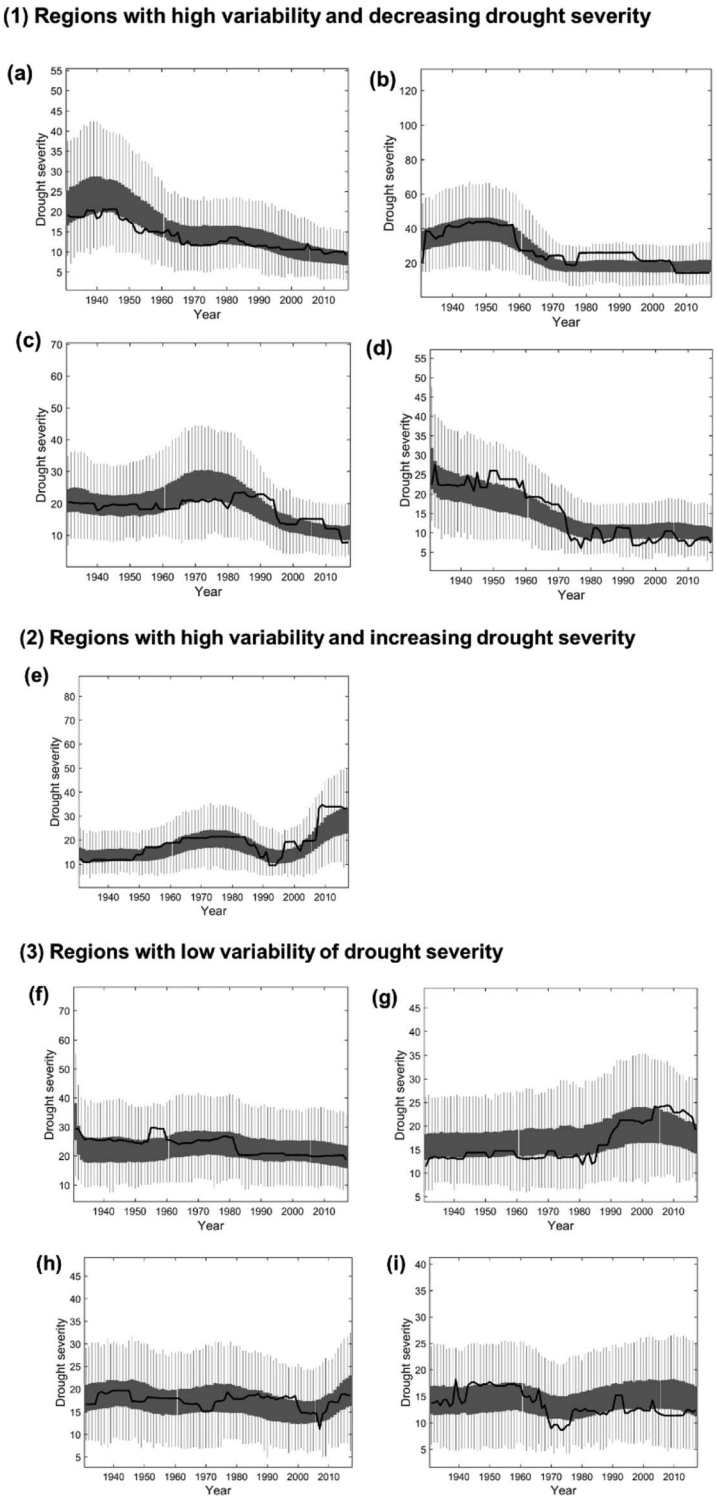

Figure 3. Observed and simulated time series of the Q95 drought severity at grid points selected from nine locations in the CONUS. Regions with high variability and decreasing drought severity: (a) Oregon and Washington, (b) Minnesota and Michigan, (c) Northeast United States, and (d) Tennessee, Nebraska, and Kansas. Regions with high variability and increasing drought severity: (e) Nevada, Utah, Arizona, and New Mexico. Regions with low variability: (f) Ohio valley; (g) Carolinas, Alabama, and Georgia; (h) California; and (i) Wyoming, eastern Colorado, and western Nebraska. The solid black lines show the observed values, the dark grey bars show the interquartile range, and light grey lines show the entire range of the Q95 severity values generated from the 1,000 simulations of the time series models. The *x* axis shows the last year of a moving window.

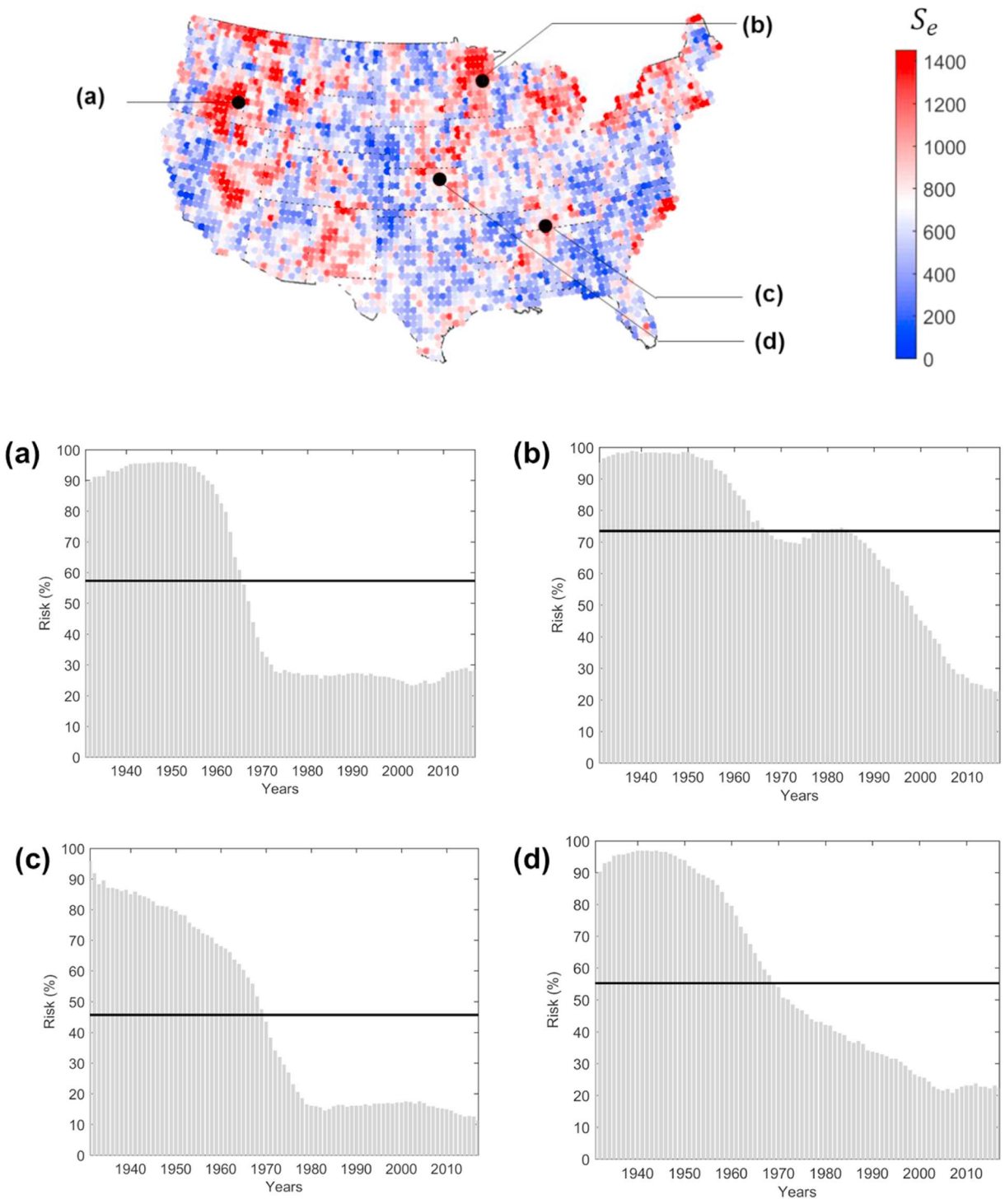

Figure 4. Stationary and nonstationary risk for locations selected from (a) Oregon, (b) Minnesota, (c) Tennessee, and (d) Kansas. Grey bars show the nonstationary risk in moving windows and the black solid line shows the risk calculated assuming stationarity, which remains constant over the observation period. The *x* axis shows the last year of a moving window.

that the multidecadal drought risk has remained quite stable in the past, because of which the nonstationary and stationary risk do not differ significantly. In California, there is an increase in the drought risk since 2007, which is evidenced by the two multiyear droughts of 2007–2009 and 2012–2016 (Figure 6a). In the Southeast United States, the drought risk has increased since the 1980s as evidenced by several severe

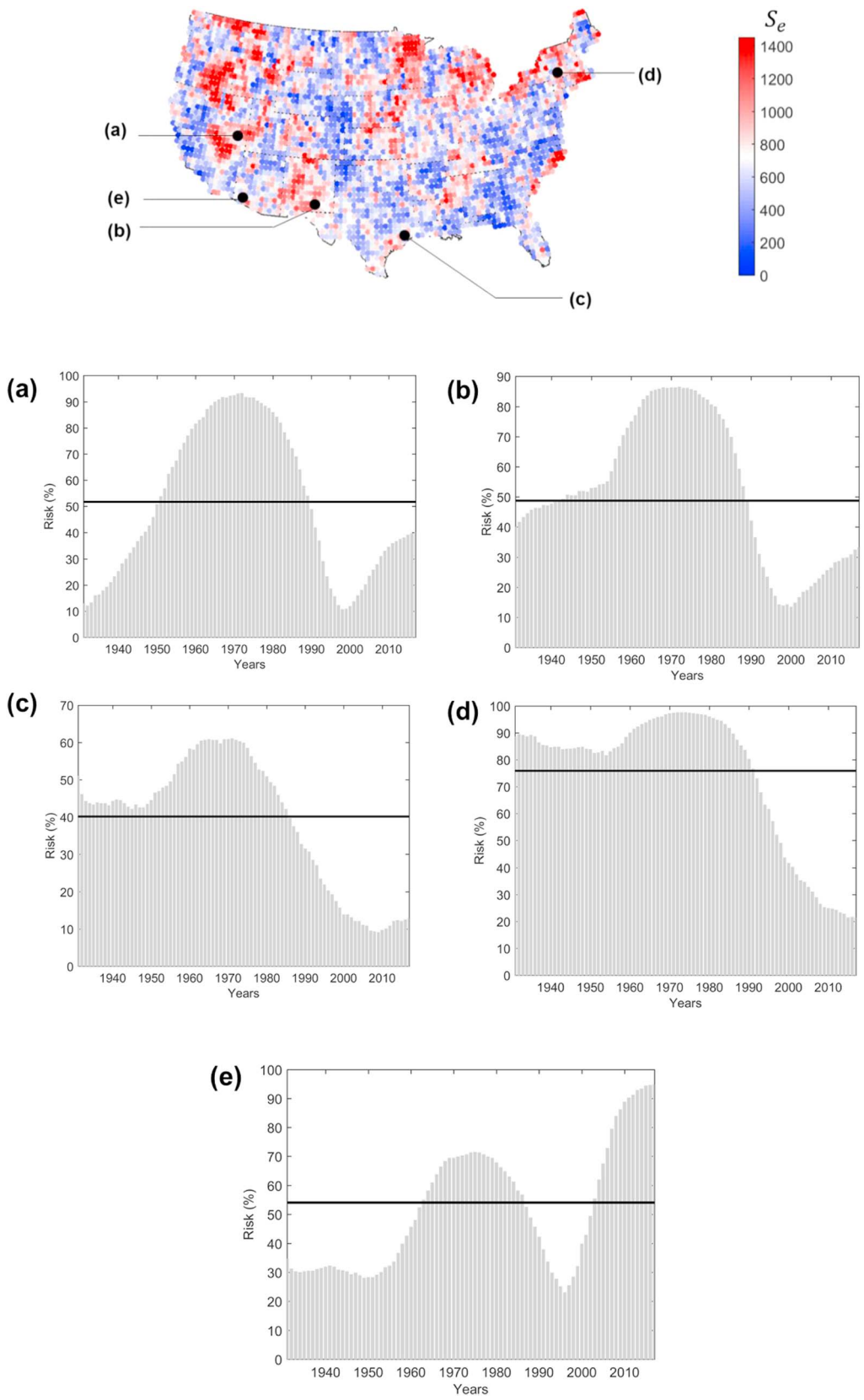

Figure 5. Stationary and nonstationary risk for locations selected from (a) Nevada, (b) New Mexico, (c) Texas, (d) Massachusetts, and (e) Arizona. The *x* axis shows the last year of a moving window.

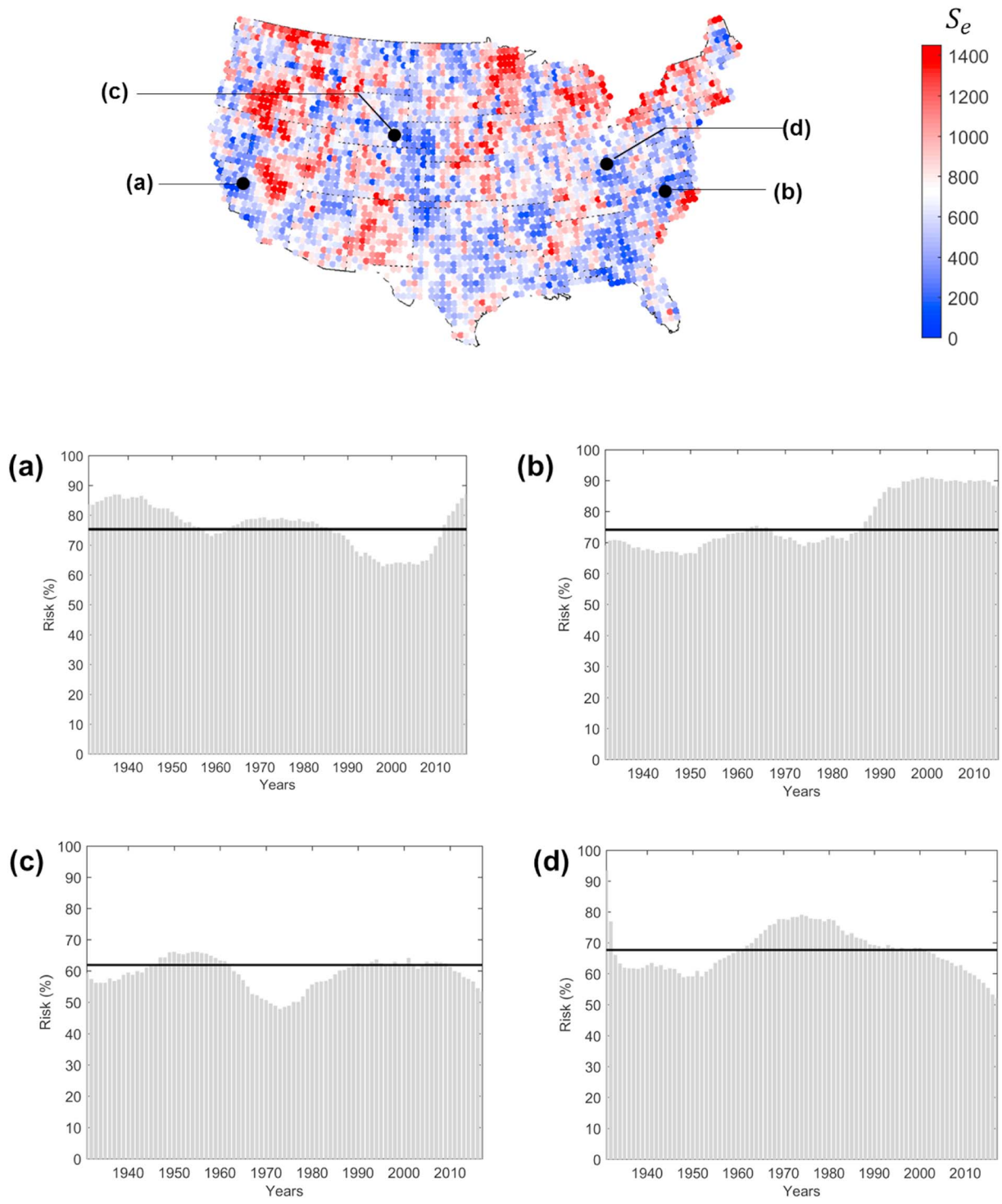

Figure 6. Stationary and nonstationary risk for locations selected from (a) California, (b) North Carolina, (c) Wyoming, and (d) Ohio. The *x* axis shows the last year of a moving window.

droughts in the last three decades (Figure 6b), including the droughts during 1986–1987, 1998–2002, and 2007–2008.

It is important to note that the number of rain gauge stations used for the development of the CRU data set has not been constant over time, which can lead to some uncertainty in the data. In order to evaluate if the

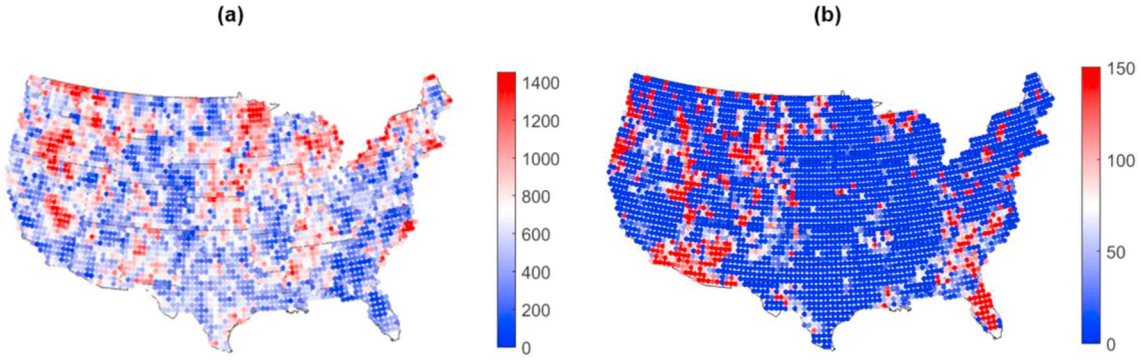

Figure 7. Spatial distribution of S_e values calculated (a) before and (b) after 1970.

uncertainty in the CRU data set has an effect on the results, we selected rain gauge stations from the United States Historical Climatology Network data set, which are located closest to the 13 grid points from the CRU data set discussed in Figures 4–6. We computed the stationary and nonstationary risk levels for these 13 rain gauge stations using the same methodology described in section 2.2. The results are shown in Figures S12–S14 in the supporting information. Comparison of the results in Figures S12–S14 with Figures 4–6 shows that the patterns of drought risk are very similar for the CRU data set and the data from the rain gauge stations. The results suggest that the uncertainty in the CRU monthly rainfall data set does not have a significant effect on the patterns of drought risk at the multidecadal scale identified in our study. The multidecadal variability of drought risk is influenced by large-scale interdecadal changes in precipitation, and these changes seem to be captured well in the CRU-TS data set. As shown in section 4.1, the multidecadal variability of drought risk is influenced by large-scale interdecadal changes in precipitation, but not so much by the changes at the monthly scale.

Finally, we disaggregate the values of S_e, calculated using the entire observation data, into two components by calculating S_e over the moving windows before and after the 1941–1970 moving window. We still use the stationary risk calculated using the entire observation for calculating the S_e values for these two periods. Figure 7 shows the spatial distribution of S_e values calculated for the two periods. As we can see, the results before 1970 (Figure 7a) are almost the same as those calculated using the entire observation period. This implies that most periods of high nonstationary drought risk in the CONUS have occurred before 1970. However, after 1970, we can observe a totally opposite spatial pattern of S_e values. Regions such as the Northwest, the upper Midwest, Nebraska, Kansas, Tennessee, and the Northeast, in which high nonstationary risk occurred before 1970, have very low S_e values after 1970. On the other hand, parts of Arizona and Southern California in the Southwest and most of the Southeast United States, which had low S_e values before 1970, show high S_e values after 1970.

3.4. Statistical Test for Detecting Changes in Drought Severity

Having analyzed the spatial and temporal changes in drought risk, we perform statistical tests to determine if the interdecadal changes in the probability distribution of drought severity have been statistically significant. For each grid point, we identify two independent (or nonoverlapping) moving windows with the maximum difference in the nonstationary drought risk in the past and compare the probability distribution functions of drought severity in these two moving windows. For example, for the location selected from Oregon, shown in Figure 4a, the moving windows with the maximum difference in the nonstationary risk are those with the last years 1941 and 1973. We then apply the two-parameter Anderson-Darling test (Anderson & Darling, 1952) to test if the distribution functions are statistically different in the periods with highest and lowest risk in the past for each grid point. Anderson-Darling (AD) test is a commonly used nonparametric test to test the null hypothesis that two samples have the same underlying distribution and has been shown to be more powerful than other nonparametric tests such as the Kolmogrov-Smirnov test and the Cramer-von Mises test (Engmann & Cousineau, 2011; Razali & Wah, 2011). The results of the AD test at 5% significance level are shown in Figure 8a. We find that the null hypothesis can be rejected at 44% of the total grid points in the CONUS (shown as the dark blue points in Figure 8a), which shows that there has been a statistically

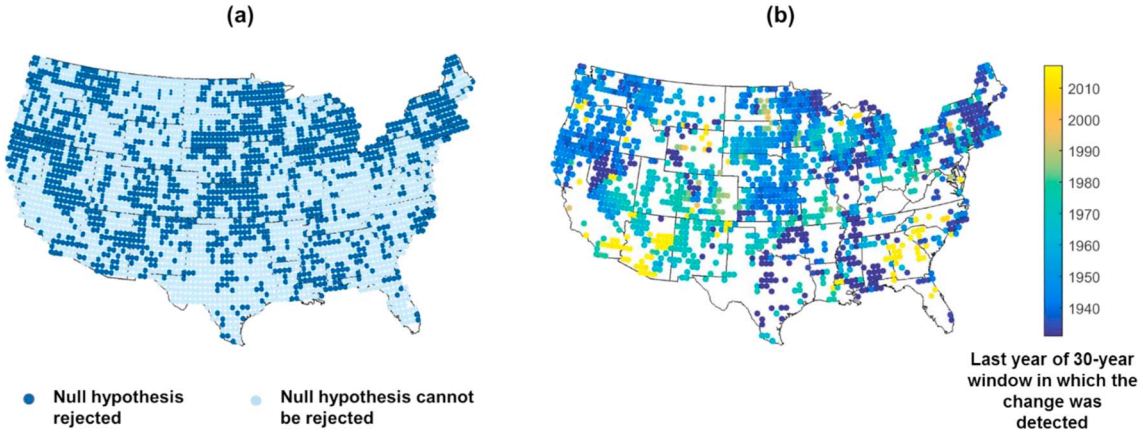

Figure 8. (a) Results of Anderson-Darling test applied to probability distribution functions of drought severity in moving windows with maximum difference in drought risk at each grid point at 5% significance level. (b) The last year of the 30-year moving window in which statistically significant change was detected in the Anderson-Darling test.

significant change in the statistical properties of droughts in the past in these regions. We can see that the null hypothesis is rejected in regions with high interdecadal variability of drought risk such as Oregon and Washington in the Northwest; Nevada, Utah, Arizona, and New Mexico in the Southwest; Nebraska, Tennessee, and Kansas in Central United States; and Minnesota and Michigan in the upper Midwest and in most of the Northeast United States. The statistically significant changes in the underlying probability distribution functions of drought severity show that the assumption of stationarity is violated in these regions of the CONUS. On the other hand, the interdecadal changes in drought severity are not statistically significant in California, the northern Plains, the Ohio valley, and the Southeast United States. Figure 8b shows the years, each of which represents the last year of the moving window in which statistically significant changes in drought severity are detected. The most significant change in drought severity is detected during the 1920–1950 period in the Northwest, Tennessee, and Kansas in Central United States and parts of Upper Midwest. In the Northeast United States, most locations show significant change in the 1951–1980 period while some locations show significantly high severity during 1901–1930. In the Southwest United States, locations in Utah, Nevada, and New Mexico show significant change during 1941–1970 whereas some locations in Arizona show statistically significant changes during 1986–2015. These results are consistent with the temporal patterns shown in Figures 4–6.

We also perform the field significance test for each state of the CONUS to evaluate the joint statistical significance of the Anderson-Darling test at individual grid points in each of the states by applying the false discovery rate criterion (Wilks, 2006). The fulfilment of the false discovery rate criterion in a given state implies that the global null hypothesis of stationarity can be rejected for the grid points lying in the state. The results of the field significance test at the field significance level of 5% are shown in Figure 9. The results show a similar pattern as that in Figure 8; that is, statistically significant nonstationarity is identified for states in the Northwest, eastern Great Plains, Upper Midwest, Northeast United States, and in some states of the Southwest United States.

4. Discussion

4.1. Causes of Nonstationarity

One of the major criticisms about nonstationary models is that these models should not be used simply because they improve the statistical representation of the observed data. Montanari and Koutsoyiannis (2014) emphasized that it is important to identify the physical mechanisms which are contributing toward the nonstationarity in the time series, before using the nonstationary models for any relevant information and decision support. Hence, in this section, we discuss the factors that have contributed toward nonstationarity in drought risk at the multidecadal scale in the CONUS.

Previous studies have shown that oscillations in SSTs in the Pacific (Hoerling & Kumar, 2003; McCabe & Dettinger, 1999) and the North Atlantic Ocean (Enfield et al., 2001) have a significant impact on the

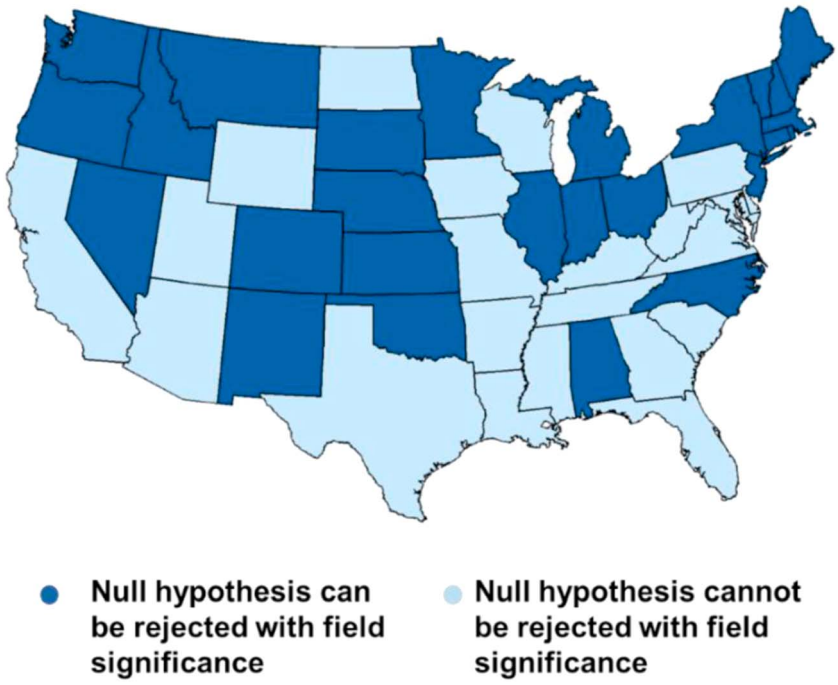

Figure 9. Results of the field significance test for the Anderson-Darling test at field significance level of 5% for each state of the CONUS.

changes in meteorological droughts in the CONUS at the decadal scale (Gray et al., 2003). The interdecadal variability of precipitation in the CONUS is modulated by the PDO and the AMO (Dettinger et al., 2001; McCabe et al., 2004). Also, the El Niño–Southern Oscillation has a significant influence on droughts in the CONUS at the annual scale (Kam et al., 2014a).

Previous studies have used statistical analysis to show that AMO, PDO, and global warming have been the most relevant factors for the multidecadal variability of droughts in the CONUS in the last 117 years (Apurv et al., 2019; McCabe et al., 2004). These studies have also shown that the northern hemisphere average temperature (NH temperature) can be used as a proxy variable to represent the influence of global warming. The time series of AMO, PDO, and NH temperature are shown in Figure 10. As the figure shows, AMO oscillates in cycles of 60–80 years, whereas PDO has cycles of 40–60 years. In Figure 10, we also plot the correlation coefficient between the nonstationary drought risk and the 30-year moving averages of AMO, PDO, and NH temperature to illustrate how these variables influence the multidecadal variability of drought risk in the CONUS. The correlation coefficients are plotted only for those grid points at which statistically significant nonstationarity is detected using the Anderson-Darling test. Statistically significant correlations at a 5% significance level are marked with black dots in Figure 10. As can be seen, AMO has positive correlation with the nonstationary drought risk in the Midwest, Great Plains, Southwest, and parts of Southeast United States (Figure 10d). PDO shows negative correlation with drought risk in the Southwest, southern Great Plains, and Northeast United States and positive correlation in the Northwest United States (Figure 10e). Global warming, represented by NH temperature, shows strong negative correlations with drought risk in the Northwest, Northeast, Midwest, and Great Plains and positive correlations in parts of Southeast and Southwest United States (Figure 10f). In summary, the results described above show how AMO, PDO, and global warming affect the nonstationary drought risk in different regions of the CONUS, as detailed in the following.

Previous studies have shown that the positive phase of AMO creates favorable conditions for droughts in the Central and Northern Great Plains and the Midwest (McCabe et al., 2004; Nigam et al., 1999, 2011), whereas the negative phase of PDO is favorable for droughts in the Southwest and the Southern Great Plains (Mantua et al., 1997; Mantua & Hare, 2002; McCabe et al., 2004). It can be seen from Figure 10a that AMO was in its positive phase during 1930–1960. Previous studies have used climate models to show that the positive phase

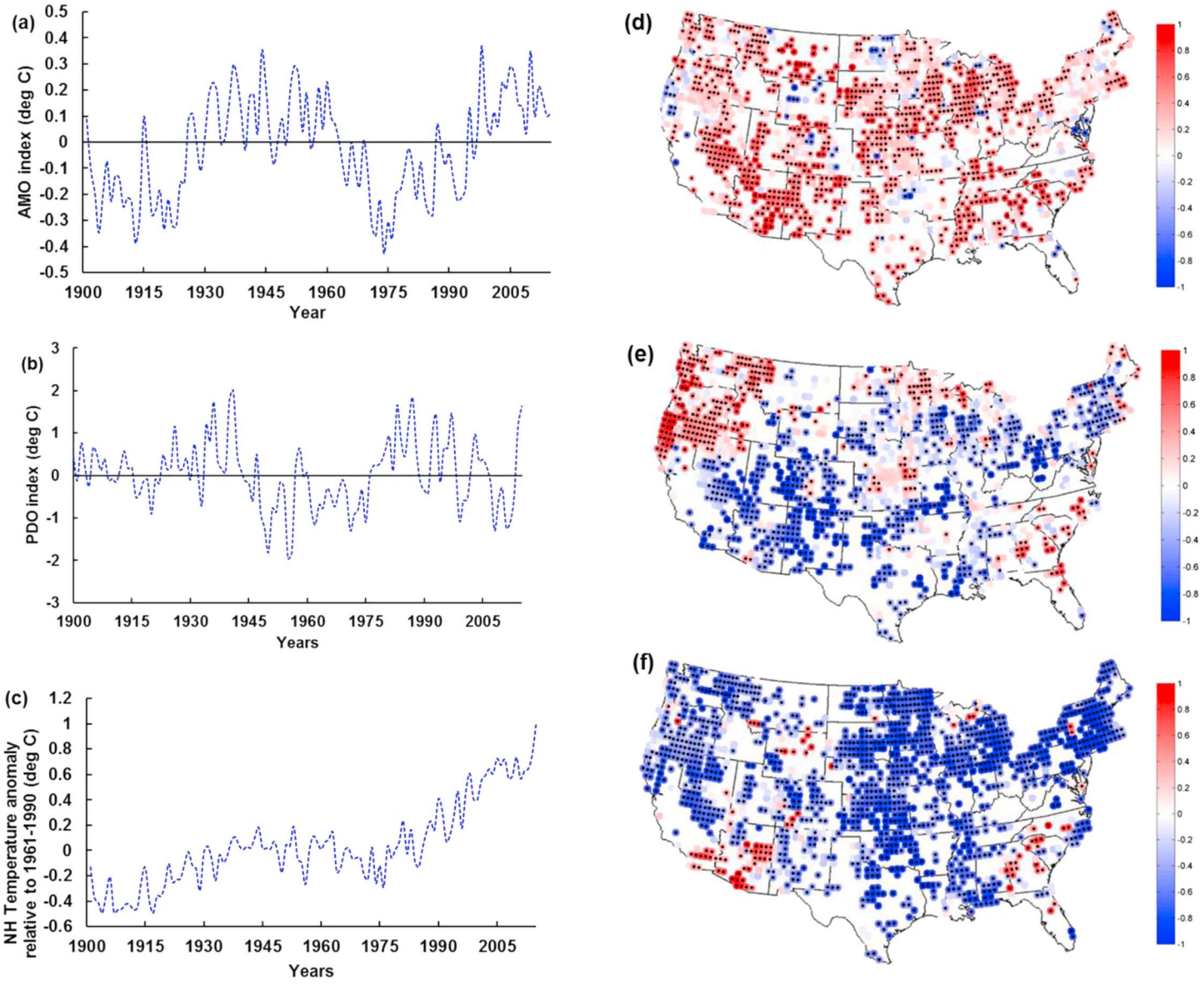

Figure 10. Time series of (a) AMO, (b) PDO, and (c) NH temperature anomaly with respect to 1961–1990, which includes temperature over both land and oceans of the northern hemisphere. Correlation coefficients between the nonstationary drought risk and 30-year moving averages of (d) AMO, (e) PDO, and (f) NH temperature for regions with statistically significant nonstationarity. Statistically significant correlations are marked with black dots ($p < 0.05$). Data sources: NOAA for AMO and PDO and CRU for NH temperature time series.

of AMO and weak La Nina conditions in the 1930s played an important role in the initiation of the 1930s drought (Schubert et al., 2004a, 2004b; Seager et al., 2008). However, other factors such as atmospheric variability, soil moisture feedback, and dust storms also played a significant role in amplifying the severity of droughts during this period (Cook et al., 2014; Hoerling et al., 2009), which ultimately resulted in high drought risk during this period in the northern parts of the CONUS including the Northwest, central and northern Great Plains, and the upper Midwest (Figure 4). During the 1950s, the AMO was in the positive phase and the PDO was in the negative phase (Figures 10a and 10b). Studies by Hoerling et al. (2009) and Schubert et al. (2004a) used climate model runs, forced with observed SSTs, to show that the positive phase of AMO and the negative phase of PDO were the dominant factors affecting the droughts in the Southwest and Southern Great Plains in the 1950s, which resulted in increased drought risk during this period in these regions (Figure 5). More recently, the shift of PDO into its negative phase in the late 1990s

has also contributed to increased droughts in the Southwest United States since the early 2000s (Kam & Sheffield, 2016; Lehner et al., 2018; Figures 5a, 5b, and 5e).

Previous studies also provide evidences for the role of global warming in the reduced drought risk after 1970 in the Northwest, the Midwest, the Great Plains, and the Northeast United States, and the aggravated risk in the Southwest and Southeast United States (Figures 7b and 10f). The increase in precipitation in the northern parts of the CONUS including the Northwest and the Midwest has been shown to be associated with earlier melting of snow in the spring season because of increasing temperatures, which in turn leads to increased formation of cumulonimbus clouds and increased summer precipitation (Groisman et al., 2004). For the Great Plains, a study by Trenberth et al. (2005) analyzed the moisture in vertical air columns and showed that increasing temperatures contributed to more precipitation in these regions through increased evaporation and increased moisture-holding capacity of the atmosphere. Meanwhile, the increase in droughts in the Southwest and the decrease in droughts in the Northeast has been found to be a result of the intensification of the dipole circulation pattern over United States, which is associated with the formation of an anomalous midtropospheric high-pressure ridge over western United States and a low-pressure trough formation over eastern United States (Singh et al., 2016). This has led to decreased precipitation in the Southwest United States but increased precipitation in the Northeast United States. Further, recent studies have attributed the intensification of the dipole pattern in recent decades to increased greenhouse gas concentration in the atmosphere (Singh et al., 2016; Wang et al., 2014; Yoon et al., 2015). In the Southeast United States, the study by Li et al. (2011) showed that the increase in the number of droughts in the last three decades is a result of the westward movement of the North Atlantic Subtropical High (NASH). NASH brings warm and humid air from the tropical Atlantic, which leads to large-scale summer precipitation in the Southeast United States (Kam et al., 2014b). However, due to the westward movement of NASH, this moisture is supplied to the Midwest region, leading to droughts in the Southeast United States. This westward movement of NASH has been attributed to the anthropogenic warming caused by greenhouse gases (Li et al., 2011). Although the study by Diem (2013) claimed that the westward movement of NASH had not been significant and that it was not influenced by global warming, several later studies have shown that the increase in drought risk in the Southeast United States is indeed linked to the intensification of NASH due to global warming (Li et al., 2013; Ryu et al., 2018; Ryu & Hayhoe, 2017). Thus, the multidecadal changes in the drought risk in the last 117 years are a result of the joint influence of multidecadal oscillation of SSTs in the Atlantic and Pacific Oceans and global warming.

4.2. Sensitivity Analysis

Different parameters such as the time scale of SPI calculation, the threshold used for defining droughts, and the design event for which the risk is calculated are selected for sensitivity analysis. We repeat the analysis for a different time scale of SPI (three months; Figure S8), for a different drought threshold −0.5 (Figure S9), and for different design events (Figures S10 and S11). The results of the analyses are shown in Figures S8–S11 in the supporting information. We find that the results in Figure 2 do not change significantly with the changes in these parameters, probably because the time scale of analysis of the changes in drought risk in this study, which is 30 years, is much larger than the time scale of drought events. The changes in drought risk at the 30-year scale are observed only when there are significant changes in precipitation at the multidecadal scale. These large changes in precipitation across decades have a significant influence on the drought events at all time scales, different threshold levels, and different magnitudes of drought events. For example, consider the location in Nevada, shown in Figure 5a, where the drought risk is very high during the 1941–1970 period. In Figure 11, we compare the time series of SPI6 and SPI3 for this location. As we can see, SPI6 is smoother than SPI3 because it considers six-month rainfall. However, if we compare two moving windows, say 1941–1970 with 1951–1980, the droughts are more severe during 1941–1970 than those during 1951–1980 for both SPI6 and SPI3. As a result, we obtain similar changes in drought risk using the 30-year moving windows for both the time scales of SPI (Figures 11c and 11d). Similarly, if we choose a different threshold for defining droughts or a different design event, the drought risk will always be higher during 1941–1970 than during 1951–1980. In summary, while using different time scales for SPI calculation, different thresholds for defining droughts, or different design events, the relative changes in the drought risk at the 30-year time scale show a similar pattern.

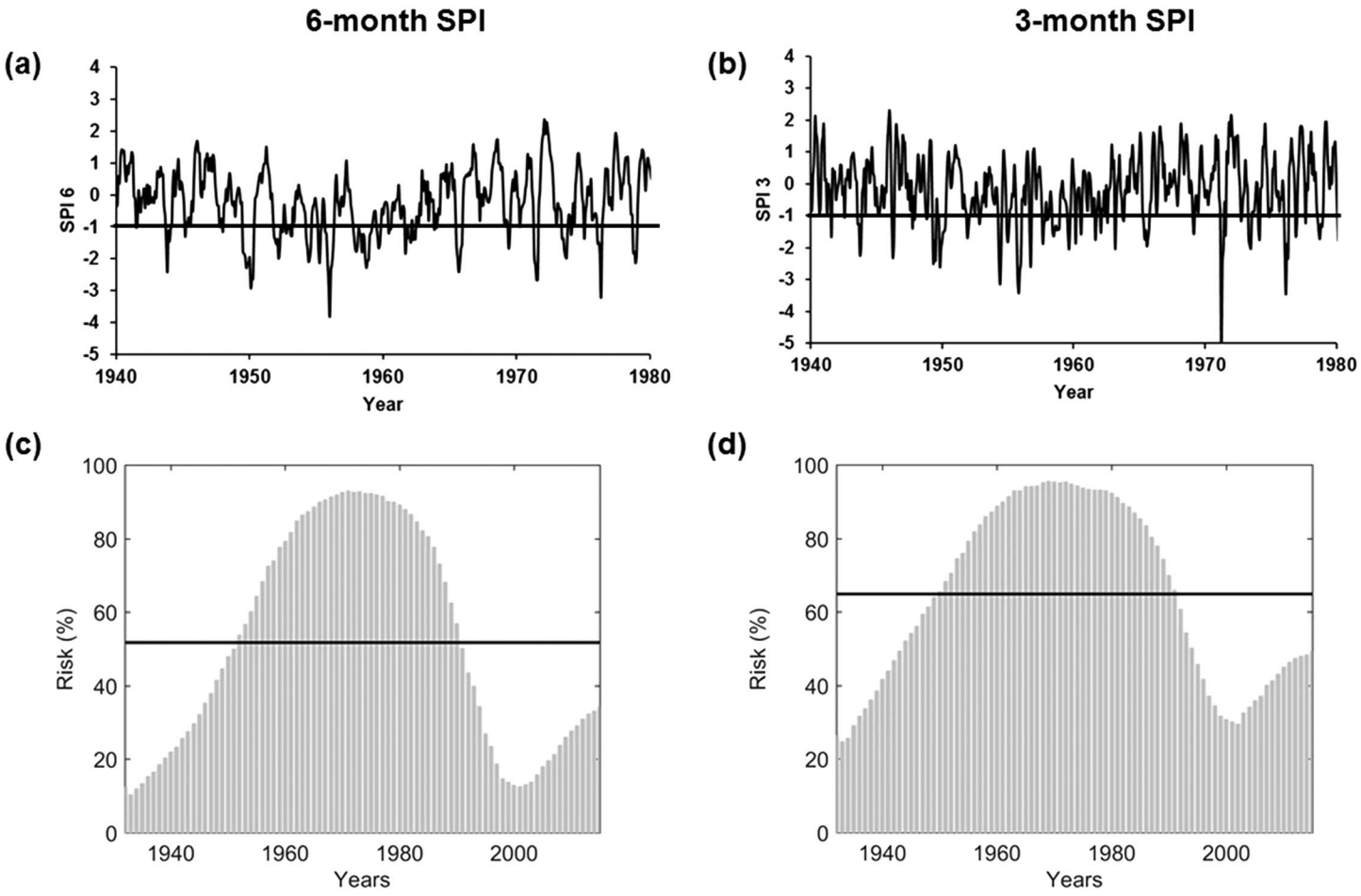

Figure 11. Time series of SPI calculated at (a) six-month and (b) three-month time scales for the grid point in Nevada. (c and d) The nonstationary risk for SPI6 and SPI3, respectively.

4.3. Implications for Drought Risk Planning and Management

We find high interdecadal variability of drought risk in parts of the Northwest, the upper Midwest, eastern parts of the Great Plains, and the Northeast United States as a result of which the nonstationary drought risk has been significantly higher than the stationary drought risk in these regions in the past (Figures 4 and 5d). For example, for the grid point selected from Oregon in the Northwest United States (Figure 4a), the nonstationary drought risk was close to 100% during 1921–1950, as compared to the risk calculated by assuming stationarity, which is around 59%. This means that it was almost certain that the design drought event S0 would be exceeded at least once during the 1921–1950 period. On the other hand, if we assume stationarity, the probability of exceedance of the design event S0 in any 30-year period is 0.59. Thus, even though the current drought risk in these regions is much lower than the stationary estimate of drought risk, the assumption of stationarity can lead to significant underestimation of drought risk in these regions if drought events of similar magnitude as the 1930s drought were to occur again. We also find high multidecadal variability of drought risk in the states of Nevada, New Mexico, Utah, and Arizona in the Southwest United States. These regions have been subjected to high nonstationary drought risk during the 1941–1970 period (Figures 5a–5c and 5e). For example, in Nevada (Figure 5a), the nonstationary risk is almost 40% higher than the stationary drought risk during the 1941–1970 period. The drought risk in the Southwest decreases in the 1980s and 1990s but starts to increase again since the year 2000 and has again exceeded the stationary estimate of risk in parts of Arizona (Figures 5e and 7b). Thus, assuming stationarity for the planning and design of water resource systems in these regions with high interdecadal variability in the climate can expose the systems to failure due to the underestimation of risk in the high-risk periods. Furthermore, the application of the Anderson-Darling test shows that there have been statistically significant interdecadal changes in the

probability distribution functions of drought severity in these regions, which indicates the violation of the stationarity assumption (Figures 8 and 9).

We find low interdecadal variability of drought risk in California along the west coast, northern and western Great Plains, the Ohio valley in the Midwest, and parts of the Southeast United States (Figure 6). In these regions, the nonstationary drought risk has remained quite stable in the last 117 years, as a result of which the estimates of risk obtained by assuming stationarity and nonstationarity are quite similar. However, there is an increase in drought risk in California in the last decade (Figure 6a). Studies have shown that the drought risk in California is expected to increase further in the future under the influence of global warming (Singh et al., 2016; Wang et al., 2014; Yoon et al., 2015). This means that the nonstationary drought risk may exceed the stationary estimate of risk in the near future in California. In the Southeast United States, the nonstationary risk has been higher than the stationary estimate of drought risk since 1980s (Figures 6b and 7b). Actually, the region has experienced three major drought events since the 1980s: the droughts of 1986–1987, 1998–2002, and 2007–2008, which is not common for this region. The increase in drought risk in this region has been shown to be a result of global warming and is expected increase further in the future (Li et al., 2012, 2013; Ryu & Hayhoe, 2017; Ryu et al., 2018). Thus, in spite of the low interdecadal variability of drought risk in the past, the assumption of stationarity for drought risk estimation may not be safe for planning and management in California and the Southeast United States in the future due to the increasing risk of droughts in these regions under the influence of global warming. Meanwhile, in parts of northern and western Great Plains and the Ohio valley, the stationarity assumption appears to be justified for estimating drought risk, since the nonstationary risk has remained stable in almost the whole observation period (Figures 6c and 6d).

5. Conclusion

In this study, we analyzed the nonstationarity of meteorological droughts at the multidecadal scale in the CONUS during 1901–2017. We used a moving window of 30 years to calculate the nonstationary drought risk and compared it with the stationary drought risk at each grid point of a high-resolution precipitation data set for the CONUS. Based on the extent of variability in the past and the ongoing changes in the nonstationary drought risk in recent decades, we evaluated in which regions of the CONUS the assumption of stationarity can be safely used for estimating drought risk for drought risk planning and management.

We find statistically significant interdecadal changes in the distribution functions of drought severity in the past in parts of the Northwest, the upper Midwest, the Northeast, eastern parts of Great Plains and in parts of Arizona, New Mexico, Nevada, and Utah in the Southwest, which leads to the violation of the assumption of stationarity in these regions. We find that in these regions, the nonstationary drought risk estimate significantly exceeds the stationary drought risk estimate in the past. Therefore, the assumption of stationarity for estimation of drought risk could lead to underestimation of drought risk in these regions, thereby making water resource systems vulnerable to failure from severe droughts. The results of our study show that a nonstationary modeling framework is required to model the high interdecadal variability in the climate of these regions. One of the possible ways of nonstationary modeling of droughts could be to use AMO and PDO as external covariates in the nonstationary models, which strongly influence the hydro-climatic variability in many of these regions such as the Southwest, the Great Plains, and the Northwest.

On the other hand, we find that the interdecadal changes in the distribution functions of drought severity are not statistically significant in California, northern and western Great Plains, the Ohio Valley, and the Southeast United States. In these regions, the drought risk estimated assuming stationarity and nonstationarity are quite similar due to the low interdecadal variability of drought risk. However, the drought risk has increased in the recent decades in the Southeast and in California, and the assumption of stationarity can lead to underestimation of drought risk in the future if the ongoing trend continues under the influence of global warming, as predicted by several recent studies. The strong role of global warming on the recent changes in the drought risk in these regions makes it important to have more accurate general circulation models that can predict the changes in the drought-relevant processes in these regions. Nonstationary models can be fit to projections from these general circulation models, which can then be used for risk estimation in the future.

The strong multidecadal variability of meteorological drought risk identified in this study highlights the necessity of conducting nonstationary risk analysis in many parts of the CONUS. The time series of

indices representing SST oscillations (AMO and PDO) and global warming (NH temperature) can be used as physical covariates for nonstationary modeling of multidecadal drought risk in the CONUS. However, the estimation of future drought risk using nonstationary models remains as a challenging task due to the uncertainties about how SST oscillations will operate in the future. Studies have shown that the current general circulation models are not good enough at capturing the multidecadal variability of AMO and PDO (Sheffield et al., 2013). This makes it difficult to project how these oscillations will evolve under global warming. Furthermore, studies have shown that CMIP5 models are unable to model the low-frequency variability and persistence of meteorological droughts (Abatzoglou & Rupp, 2017; Ault et al., 2012, 2013; Cheung et al., 2017; Moon et al., 2018). Thus, improved representation of the physical processes influencing the multidecadal variability of droughts in climate models is crucial for successful implementation of nonstationary models for risk analysis in the future.

Under uncertain future drought conditions, bottom-up approaches (e.g., Brown et al., 2012; Lempert et al., 2004; Prudhomme et al., 2010) can be useful for planning and management of water resource systems in regions with significant multidecadal nonstationarity in the past. The focus of bottom-up approaches is to ensure satisfactory performance of water resource systems over a wide range of plausible climate scenarios, rather than relying on a limited number of future projections. The bottom-up approaches can be used for testing the performance of water resource systems over a wide range of drought risk levels observed in the past, as well as those projected for the future. Stochastic simulations of meteorological droughts from different periods (e.g., 30 years), with varying levels of drought risk in the past, can be used for generating precipitation scenarios as inputs for water resource system models. For example, for the location selected from Oregon (in Figure 4a), simulation of precipitation time series based on the 1921–1950 period can be used as a "high drought risk" scenario, whereas 1988–2017 can be used as a "low drought risk" scenario. The parameters of time series models can be further altered to generate more severe drought conditions than those observed in the past.

Another limitation of our study is that while we have focused on meteorological droughts, the water availability during droughts is determined by the joint impact of precipitation and temperature during drought events. Many recent studies have shown that high temperatures during drought events can significantly exacerbate the impact of droughts (AghaKouchak et al., 2014; Diffenbaugh et al., 2015), and hence, the analysis of meteorological droughts presented in this study does not fully represent the risk posed by droughts to water resource systems. Increase in temperatures due to global warming can introduce nonstationarity in the drought risk even if the meteorological drought risk remains stationary. Therefore, in future studies, the joint analysis of temperature and precipitation time series should be used to evaluate the nonstationary of drought risk.

Appendix A

This appendix describes the procedure for the disaggregation of the annual precipitation time series into monthly values using the nonparametric approach developed by Prairie et al. (2007).

The disaggregation procedure involves sampling from conditional probability density function f($\mathbf{x}$| Z), where $\mathbf{x}$ is a "d" dimensional vector of monthly precipitation (d = 12) and Z is the annual precipitation. The elements of x should add up to Z. This procedure involves the following steps:

1. First, a matrix $\mathbf{X}$ needs to be created, in which the rows correspond to monthly precipitation values and the columns correspond to the years. Thus, the matrix $\mathbf{X}$ has dimensions $d \times T$, where T is the number of years.
2. The second step is to create an orthonormal rotation matrix $\mathbf{R}$ with dimensions $d \times d$. The matrix can be obtained by setting the last row of d dimensional identity matrix as the vector $\left[\frac{1}{\sqrt{d}}, \frac{1}{\sqrt{d}}, \ldots\ldots\ldots, \frac{1}{\sqrt{d}}\right]$ and then applying Gram Schmidt orthonormalization procedure to the remaining $d - 1$ rows. The details of this step can be found in Tarboton et al. (1998).
3. The third step is to rotate the monthly rainfall time series $\mathbf{X}$ into $\mathbf{Y}$ by multiplying it with the rotation matrix R. Both $\mathbf{X}$ and $\mathbf{Y}$ have the same dimensions.

$$\mathbf{Y} = \mathbf{RX} \tag{10}$$

The last row of the matrix $\mathbf{Y}$ is $Y_d = \frac{Z}{\sqrt{d}} = Z'$. If the first $d-1$ rows of the matrix $\mathbf{Y}$ are denoted by $\mathbf{U}$, then the matrix $\mathbf{Y}$ can be denoted as $Y = (\boldsymbol{U}, Z')$.

4. Let us assume that the annual precipitation obtained from GAMLSS simulation is Z_{sim}. One of the K nearest neighbors of Z_{sim} in the historical record is resampled using the following weight function:

$$w(k) = \frac{1}{k\sum_{i=1}^{K} 1/i} \tag{11}$$

where $k = 1,2 \ldots K$. This weight function gives higher weights to nearer neighbors and less weights to farther neighbors. Lall and Sharma (1996) suggested that the number of nearest neighbors $K = \sqrt{N}$, where N is the sample size of historical record. Let j be the index of the year (column in matrix $\mathbf{Y}$) selected as the nearest neighbor in KNN resampling.

5. The j^{th} column of the matrix $\mathbf{Y}$ is then modified as

$$Y^* = \left(U_j, Z_{sim}\right) \tag{12}$$

The final step is back rotation of Y* into the original space

$$X^* = \boldsymbol{R}^T Y^* \tag{13}$$

X* is the desired vector containing the disaggregated monthly precipitation values.

A more detailed description of the methodology can be found in Prairie et al. (2007).

Acknowledgments
We are grateful for the financial support for this study by the Institute for Sustainability, Energy and Environment (iSEE), University of Illinois Urbana–Champaign. The study uses the Climate Research Unit monthly rainfall data set (CRU TS4.02) that has a 0.5° spatial resolution and covers the period 1901 to 2017. GAMLSS modeling was performed using the GAMLSS package (Stasinopoulos & Rigby, 2007) in the software R. The monthly time series of AMO was obtained from the National Oceanic and Atmospheric Administration (NOAA) website (https://www.esrl.noaa.gov/psd/data/timeseries/AMO), the monthly time series of PDO was also obtained from the NOAA website (https://www.ncdc.noaa.gov/teleconnections/pdo), and the NH average temperature data were taken from the CRU data set (www.cru.uea.ac.uk/cru/data/temperature).

References

Abatzoglou, J. T., & Rupp, D. E. (2017). Evaluating climate model simulations of drought for the northwestern United States. *International Journal of Climatology*, *37*, 910–920. https://doi.org/10.1002/joc.5046

AghaKouchak, A., Cheng, L., Mazdiyasni, O., & Farahmand, A. (2014). Global warming and changes in risk of concurrent climate extremes: Insights from the 2014 California drought. *Geophysical Research Letters*, *41*, 8847–8852. https://doi.org/10.1002/2014GL062308

Ahn, K. H., & Palmer, R. N. (2016). Use of a nonstationary copula to predict future bivariate low flow frequency in the Connecticut river basin. *Hydrological Processes*, *30*(19), 3518–3532. https://doi.org/10.1002/hyp.10876

Akaike, H. (1974). A new look at the statistical model identification, *IEEE trans. Autom. Control 19*(6), 716–723. https://doi.org/10.1109/TAC.1974.1100705

Anderson, T. W., & Darling, D. A. (1952). Asymptotic theory of certain "goodness of fit" criteria based on stochastic processes. *Annals of Mathematical Statistics*, *23*(2), 193–212. https://doi.org/10.1214/aoms/1177729437

Apurv, T., Cai, X., & Yuan, X. (2019). Influence of internal variability and global warming on multidecadal changes in regional drought severity over the continental U.S. *Journal of Hydrometeorology*, *20*(3), 411–429. https://doi.org/10.1175/JHM-D-18-0167.1

Archfield, S. A., Hirsch, R. M., Viglione, A., & Blöschl, G. (2016). Fragmented patterns of flood change across the United States. *Geophysical Research Letters*, *43*, 10,232–10,239. https://doi.org/10.1002/2016GL070590

Ault, T. R., Cole, J. E., & George, S. S. (2012). The amplitude of decadal to multidecadal variability in precipitation simulated by state-of-the-art climate models. *Geophysical Research Letters*, *39*, L21705. https://doi.org/10.1029/2012GL053424

Ault, T. R., Cole, J. E., Overpeck, J. T., Pederson, G. T., George, S. S., Otto-Bliesner, B., et al. (2013). The continuum of hydroclimate variability in Western North America during the Last Millennium. *Journal of Climate*, *26*(16), 5863–5878. https://doi.org/10.1175/JCLI-D-11-00732.1

Box, G. E. P., & Jenkins, G. (1976). *Time Series Analysis: Forecasting and Control*. San Francisco CA: Holden-Day.

Bracken, C., Holman, K. D., Rajagopalan, B., & Moradkhani, H. (2018). A Bayesian hierarchical approach to multivariate nonstationary hydrologic frequency analysis. *Water Resources Research*, *54*, 243–255. https://doi.org/10.1002/2017WR020403

Bracken, C., Rajagopalan, B., & Prairie, J. (2010). A multisite seasonal ensemble streamflow forecasting technique. *Water Resources Research*, *46*, W03532. https://doi.org/10.1029/2009WR007965

Bras, R. L., & Rodriguez-Iturbe, I. (1985). *Random Functions and Hydrology*. Reading, MA: Addison-Wesley.

Brown, C., Ghile, Y., Laverty, M., & Li, K. (2012). Decision scaling: Linking bottom-up vulnerability analysis with climate projections in the water sector. *Water Resources Research*, *48*, W09537. https://doi.org/10.1029/2011WR011212

Burke, E. J., Perry, R. H., & Brown, S. J. (2010). An extreme value analysis of UK drought and projections of change in the future. *Journal of Hydrology*, *388*(1-2), 131–143. https://doi.org/10.1016/j.jhydrol.2010.04.035

Cai, X., Zeng, R., Kang, W. H., Song, J., & Valocchi, A. J. (2015). Strategic planning for drought mitigation under climate change. *Journal of Water Resources Planning and Management*, *141*(9), 04015004. https://doi.org/10.1061/(ASCE)WR.1943-5452.0000510

Chebana, F., Ouarda, T. B. M. J., & Duong, T. C. (2013). Testing for multivariate trends in hydrologic frequency analysis. *Journal of Hydrology*, *486*, 519–530. https://doi.org/10.1016/j.jhydrol.2013.01.007

Cheng, L., & AghaKouchak, A. (2014). Nonstationary precipitation intensity-duration-frequency curves for infrastructure design in a changing climate. *Scientific Reports*, *4*, 7093.

Cheung, A. H., Mann, M. E., Steinman, B. A., Frankcombe, L. M., England, M. H., & Miller, S. K. (2017). Comparison of low-frequency internal climate variability in CMIP5 models and observations. *Journal of Climate*, *30*(12), 4763–4776. https://doi.org/10.1175/JCLI-D-16-0712.1

Chow, V. T. (1964). *Handbook of Applied Hydrology*. New York: McGraw-Hill.

Chun, K. P., Wheater, H., & Onof, C. (2013). Prediction of the impact of climate change on drought: An evaluation of six UK catchments using two stochastic approaches. *Hydrological Processes*, *27*(11), 1600–1614. https://doi.org/10.1002/hyp.9259

Coe, R., & Stern, R. (1982). Fitting models to daily rainfall. *Journal of Applied Meteorology*, *21*(7), 1024–1031. https://doi.org/10.1175/1520-0450(1982)021<1024:FMTDRD>2.0.CO;2

Cook, B. I., Seager, R., & Smerdon, J. E. (2014). The worst North American drought year of the last millennium: 1934. *Geophysical Research Letters*, *41*, 7298–7305. https://doi.org/10.1002/2014GL061661

Dettinger, M. D., Battisti, D. S., Garreaud, R. D., McCabe, G. J., & Bitz, C. M. (2001). Interhemispheric effects of interannual and decadal ENSO like climate variations on the Americas. In V. Markgraf (Ed.), *Interhemispheric Climate Linkages*, (pp. 1–16). San Diego, Calif: Academic.

Diem, J. E. (2013). Comments on "Changes to the North Atlantic Subtropical High and its role in the intensification of summer rainfall variability in the southeastern United States". *Journal of Climate*, *26*(2), 679–682. https://doi.org/10.1175/JCLI-D-11-00390.1

Diffenbaugh, N. S., Swain, D. L., & Touma, D. (2015). Anthropogenic warming has increased drought risk in California. *Proceedings of the National Academy of Sciences of the United States of America*, *112*(13), 3931–3936. https://doi.org/10.1073/pnas.1422385112

Do, H. X., Westra, S., & Leonard, M. (2017). A global-scale investigation of trends in annual maximum streamflow. *Journal of Hydrology*, *552*, 28–43. https://doi.org/10.1016/j.jhydrol.2017.06.015

Du, T., Xiong, L., Xu, C.-Y., Gippel, C. J., Guo, S., & Liu, P. (2015). Return period and risk analysis of nonstationary low-flow series under climate change. *Journal of Hydrology*, *527*, 234–250. https://doi.org/10.1016/j.jhydrol.2015.04.041

Enfield, D. B., Mestas-Nunez, A. M., & Trimble, P. J. (2001). The Atlantic multidecadal oscillation and its relation to rainfall and river flows in the continental U.S. *Geophysical Research Letters*, *28*(10), 2077–2080. https://doi.org/10.1029/2000GL012745

Engmann, S., & Cousineau, D. (2011). Comparing distributions: The two-sample Anderson-Darling test as an alternative to the Kolmogorov-Smirnoff test. *Journal of Applied Quantitative Methods*, *6*, 1–17.

Ghosh, S., Das, D., Kao, S.-C., & Ganguly, A. R. (2012). Lack of uniform trends but increasing spatial variability in observed Indian rainfall extremes. *Nature Climate Change*, *2*(2), 86–91. https://doi.org/10.1038/nclimate1327

Gilroy, K. L., & McCuen, R. H. (2012). A nonstationary flood frequency analysis method to adjust for future climate change and urbanization. *Journal of Hydrology*, *414-415*, 40–48. https://doi.org/10.1016/j.jhydrol.2011.10.009

Gray, S. T., Betancourt, J. L., Fastie, C. L., & Jackson, S. T. (2003). Patterns and sources of multidecadal oscillations in drought-sensitive tree-ring records from the central and southern Rocky Mountains. *Geophysical Research Letters*, *30*(6), 1316. https://doi.org/10.1029/2002GL016154

Groisman, P. Y., Knight, R. W., Karl, T. R., Easterling, D. R., Sun, B., & Lawrimore, J. H. (2004). Contemporary changes of the hydrological cycle over the contiguous United States: Trends derived from in situ observations. *Journal of Hydrometeorology*, *5*(1), 64–85. https://doi.org/10.1175/1525-7541(2004)005<0064:CCOTHC>2.0.CO;2

Guttman, N. B. (1989). Statistical descriptors of climate. *Bulletin of the American Meteorological Society*, *70*(6), 602–607. https://doi.org/10.1175/1520-0477(1989)070<0602:SDOC>2.0.CO;2

Guttman, N. B., Hosking, J. R. M., & Wallis, J. R. (1993). Regional precipitation quantile values for the continental United States computed from L-moments. *Journal of Climate*, *6*(2), 326–2,340. https://doi.org/10.1175/1520-0442(1993)006<2326:RPQVFT>2.0.CO;2

He, X., Wada, Y., Wanders, N., & Sheffield, J. (2017). Human water management intensifies hydrological drought in California. *Geophysical Research Letters*, *44*, 1777–1785. https://doi.org/10.1002/2016GL071665

Hoerling, M., & Kumar, A. (2003). The perfect ocean for drought. *Science*, *299*(5607), 691–694. https://doi.org/10.1126/science.1079053

Hoerling, M., Quan, X.-W., & Eischeid, J. (2009). Distinct causes for two principal U.S. droughts of the 20th century. *Geophysical Research Letters*, *36*, L19708. https://doi.org/10.1029/2009GL039860

Ishak, E., Rahman, A., Westra, S., Sharma, A., & Kuczera, G. (2013). Evaluating the nonstationarity of Australian annual maximum flood. *Journal of Hydrology*, *494*, 134–145. https://doi.org/10.1016/j.jhydrol.2013.04.021

Jain, S., & Lall, U. (2001). Floods in a changing climate: Does the past represent the future? *Water Resources Research*, *37*(12), 3193–3205. https://doi.org/10.1029/2001WR000495

Jiang, C., Xiong, L., Xu, C. Y., & Guo, S. (2015). Bivariate frequency analysis of nonstationary low-flow series based on the time-varying copula. *Hydrological Processes*, *29*(6), 1521–1534. https://doi.org/10.1002/hyp.10288

Joseph, E. S. (1970). Frequency of design drought. *Water Resources Research*, *6*(4), 1199–1201. https://doi.org/10.1029/WR006i004p01199

Kalra, A., & Ahmad, S. (2011). Evaluating changes and estimating seasonal precipitation for the Colorado River Basin using a stochastic nonparametric disaggregation technique. *Water Resources Research*, *47*, W05555. https://doi.org/10.1029/2010WR009118

Kam, J., & Sheffield, J. (2016). Increased drought and pluvial risk over California due to changing oceanic condition. *Journal of Climate*, *29*(22), 8269–8279. https://doi.org/10.1175/JCLI-D-15-0879.1

Kam, J., Sheffield, J., & Wood, E. F. (2014a). Changes in drought risk over the contiguous United States (1901–2012): The influence of the Pacific and Atlantic Oceans. *Geophysical Research Letters*, *41*, 5897–5903. https://doi.org/10.1002/2014GL060973

Kam, J., Sheffield, J., & Wood, E. F. (2014b). A multi-scale analysis of drought and pluvial mechanisms for the southeastern United States. *Journal of Geophysical Research: Atmospheres*, *119*, 7348–7367. https://doi.org/10.1002/2014JD021453

Kao, S.-C., & Ganguly, A. R. (2011). Intensity, duration, and frequency of precipitation extremes under 21st-century warming scenarios. *Journal of Geophysical Research*, *116*, D16119. https://doi.org/10.1029/2010JD015529

Katz, R. W., & Parlange, M. B. (1998). Overdispersion phenomenon in stochastic modeling of precipitation. *Journal of Climate*, *11*(4), 591–601. https://doi.org/10.1175/1520-0442(1998)011<0591:OPISMO>2.0.CO;2

Katz, R. W., Parlange, M. B., & Naveau, P. (2002). Statistics of extremes in hydrology. *Advances in Water Resources*, *25*(8–12), 1287–1304. https://doi.org/10.1016/S0309-1708(02)00056-8

Koutsoyiannis, D. (1999). Optimal decomposition of covariance matrices for multivariate stochastic models in hydrology. *Water Resources Research*, *35*(4), 1219–1229. https://doi.org/10.1029/1998WR900093

Koutsoyiannis, D. (2001). Coupling stochastic models of different timescales. *Water Resources Research*, *37*(2), 379–391. https://doi.org/10.1029/2000WR900200

Kumar, D. N., Lall, U., & Peterson, M. R. (2000). Multisite disaggregation of monthly to daily streamflow. *Water Resources Research*, *36*(7), 1823–1833. https://doi.org/10.1029/2000WR900049

Kwon, H.-H., & Lall, U. (2016). A copula-based nonstationary frequency analysis for the 2012–2015 drought in California. *Water Resources Research*, *52*, 5662–5675. https://doi.org/10.1002/2016WR018959

Kwon, H.-H., Lall, U., & Khalil, A. F. (2007). Stochastic simulation model for nonstationary time series using an autoregressive wavelet decomposition: Applications to rainfall and temperature. *Water Resources Research*, *43*, W05407. https://doi.org/10.1029/2006WR005258

Kwon, H.-H., Lall, U., & Kim, S.-J. (2016). The unusual 2013–2015 drought in South Korea in the context of a multicentury precipitation record: Inferences from a nonstationary, multivariate, Bayesian copula model. *Geophysical Research Letters*, *43*, 8534–8544. https://doi.org/10.1002/2016GL070270

Lall, U., & Sharma, A. (1996). A nearest neighbor bootstrap for resampling hydrologic time series. *Water Resources Research*, *32*(3), 679–693. https://doi.org/10.1029/95WR02966

Lehner, F., Deser, C., Simpson, I. R., & Terray, L. (2018). Attributing the U.S. Southwest's recent shift into drier conditions. *Geophysical Research Letters*, *45*, 6251–6261. https://doi.org/10.1029/2018GL078312

Lempert, R., Nakicenovic, N., Sarewitz, D., & Schlesinger, M. (2004). Characterizing climate-change uncertainties for decision-makers. An editorial essay. *Climatic Change*, *65*(1/2), 1–9. https://doi.org/10.1023/B:CLIM.0000037561.75281.b3

Li, L., Li, W., & Deng, Y. (2013). Summer rainfall variability over the southeastern United States and its intensification in the 21st century as assessed by CMIP5 models. *Journal of Geophysical Research: Atmospheres*, *118*, 340–354. https://doi.org/10.1002/jgrd.50136

Li, L., Li, W., & Kushnir, Y. (2012). Variation of the North Atlantic Subtropical High western ridge and its implication to southeastern US summer precipitation. *Climate Dynamics*, *39*(6), 1401–1412. https://doi.org/10.1007/s00382-011-1214-y

Li, W., Li, L., Fu, R., Deng, Y., & Wang, H. (2011). Changes to the North Atlantic Subtropical High and its role in the intensification of summer rainfall variability in the southeastern United States. *Journal of Climate*, *24*(5), 1499–1506. https://doi.org/10.1175/2010JCLI3829.1

Lima, C. H., Lall, U., Troy, T. J., & Devineni, N. (2015). A climate informed model for nonstationary flood risk prediction: Application to Negro River at Manaus, Amazonia. *Journal of Hydrology*, *522*, 594–602. https://doi.org/10.1016/j.jhydrol.2015.01.009

Loaiciga, H. A. (2005). On the probability of droughts: The compound renewal model. *Water Resources Research*, *41*, W01009. https://doi.org/10.1029/2004WR003075

López, J., & Francés, F. (2013). Non-stationary flood frequency analysis in continental Spanish rivers, using climate and reservoir indices as external covariates. *Hydrology and Earth System Sciences*, *17*(8), 3189–3203. https://doi.org/10.5194/hess-17-3189-2013

Lu, Y., Qin, X. S., & Xie, Y. J. (2016). An integrated statistical and data-driven framework for supporting flood risk analysis under climate change. *Journal of Hydrology*, *533*, 28–39. https://doi.org/10.1016/j.jhydrol.2015.11.041

Mallakpour, I., & Villarini, G. (2015). The changing nature of flooding across the central United States. *Nature Climate Change*, *5*(3), 250–254. https://doi.org/10.1038/nclimate2516

Mantua, N., Hare, S., Zhang, Y., Wallace, J., & Francis, R. (1997). A Pacific Interdecadal Climate Oscillation with impacts on salmon production. *Bulletin of the American Meteorological Society*, *78*(6), 1069–1079. https://doi.org/10.1175/1520-0477(1997)078<1069:APICOW>2.0.CO;2

Mantua, N. J., & Hare, S. R. (2002). The Pacific Decadal Oscillation. *Journal of Oceanography*, *58*(1), 35–44. https://doi.org/10.1023/A:1015820616384

Markovic, R. D. (1965). Probability of best fit to distributions of annual precipitation and runoff. Hydro. Paper no. 8, Colorado State Univ., Fort Collins, Colorado, USA

McCabe, G. J., & Dettinger, M. D. (1999). Decadal variations in the strength of ENSO teleconnections with precipitation in the western United States. *International Journal of Climatology*, *19*, 1,069–1,079.

McCabe, G. J., Palecki, M. A., & Betancourt, J. L. (2004). Pacific and Atlantic Ocean influences on multidecadal drought frequency in the United States. *Proceedings of the National Academy of Sciences of the United States of America*, *101*(12), 4136–4141. https://doi.org/10.1073/pnas.0306738101

McKee, T. B., Doesken, N. J., & Kleist, J. (1993). The relationship of drought frequency and duration to time scale. In *Proceedings of the Eighth Conference on Applied Climatology, Anaheim, California*, (pp. 179–184). Boston: American Meteorological Society.

Mehrotra, R., & Sharma, A. (2007). A semi-parametric model for stochastic generation of multi-site daily rainfall exhibiting low-frequency variability. *Journal of Hydrology*, *335*(1–2), 180–193. https://doi.org/10.1016/j.jhydrol.2006.11.011

Mejia, J. M., & Rousselle, J. (1976). Disaggregation models in hydrology revisited. *Water Resources Research*, *12*(2), 185–186. https://doi.org/10.1029/WR012i002p00185

Milly, P. C. D., Betancourt, J., Falkenmark, M., Hirsch, R. M., Kundzewicz, Z. W., Lettenmaier, D. P., & Stouffer, R. J. (2008). Stationarity is dead: Whither water management? *Science*, *319*(5863), 573–574. https://doi.org/10.1126/science.1151915

Milly, P. C. D., Betancourt, J., Falkenmark, M., Hirsch, R. M., Kundzewicz, Z. W., Lettenmaier, D. P., et al. (2015). On critiques of "Stationarity is dead: Whither water management?". *Water Resources Research*, *51*, 7785–7789. https://doi.org/10.1002/2015WR017408

Mondal, A., & Mujumdar, P. P. (2015). Return levels of hydrologic droughts under climate change. *Advances in Water Resources*, *75*, 67–79. https://doi.org/10.1016/j.advwatres.2014.11.005

Montanari, A., & Koutsoyiannis, D. (2014). Modeling and mitigating natural hazards: Stationarity is immortal! *Water Resources Research*, *50*, 9748–9756. https://doi.org/10.1002/2014WR016092

Moon, H., Gudmundssonand, L., & Seneviratne, S. I. (2018). Drought persistence errors in global climate models. *Journal of Geophysical Research: Atmospheres*, *123*, 3483–3496. https://doi.org/10.1002/2017JD027577

Namias, J. (1966). Nature and possible causes of the northeastern United States drought during 1962–65. *Monthly Weather Review*, *94*(9), 543–554. https://doi.org/10.1175/1520-0493(1966)094<0543:NAPCOT>2.3.CO;2

Nigam, S., Barlow, M., & Berbery, E. H. (1999). Pacific decadal SST variability: Impact on U.S. drought and streamflow. *Eos, Transactions of the American Geophysical Union*, *80*(51), 621–625. https://doi.org/10.1029/99EO00412

Nigam, S., Guan, B., & Ruiz-Barradas, A. (2011). Key role of the Atlantic Multidecadal Oscillation in 20th century drought and wet periods over the Great Plains. *Geophysical Research Letters*, *38*, L16713. https://doi.org/10.1029/2011GL048650

National Ocean and Atmospheric Administration. (2016). Billion-dollar weather and climate disasters: Table of events. Retrieved from: https://www.ncdc.noaa.gov/billions/events

Osorio, J. D. G., & Galiano, S. G. G. (2012). Non-stationary analysis of dry spells in monsoon season of Senegal River Basin using data from Regional Climate Models (RCMs). *Journal of Hydrology*, *450-451*, 82–92. https://doi.org/10.1016/j.jhydrol.2012.05.029

Prairie, J., Rajagopalan, B., Lall, U., & Fulp, T. (2007). A stochastic nonparametric technique for space-time disaggregation of streamflows. *Water Resources Research*, *43*, W03432. https://doi.org/10.1029/2005WR004721

Prosdocimi, I., Kjeldsen, T. R., & Miller, J. D. (2015). Detection and attribution of urbanization effect on flood extremes using nonstationary flood-frequency models. *Water Resources Research*, *51*, 4244–4262. https://doi.org/10.1002/2015WR017065

Prudhomme, C., Wilby, R. L., Crooks, S., Kay, A. L., & Reynard, N. S. (2010). Scenario neutral approach to climate change impact studies: Application to flood risk. *Journal of Hydrology*, *390*(3–4), 198–209. https://doi.org/10.1016/j.jhydrol.2010.06.043

Qi, W. (2017). A non-stationary cost-benefit analysis approach for extreme flood estimation to explore the nexus of 'risk, cost and non-stationarity'. *Journal of Hydrology*, *554*, 128–136. https://doi.org/10.1016/j.jhydrol.2017.09.009

Rajagopalan, B., & Lall, U. (1999). A k-nearest-neighbor simulator for daily precipitation and other weather variables. *Water Resources Research*, *35*(10), 3089–3101. https://doi.org/10.1029/1999WR900028

Rajagopalan, B., Salas, J. D., & Lall, U. (2010). Stochastic methods for modeling precipitation and streamflow. In *Advances in Data-Based Approaches for hydrologic Modeling and Forecasting*, (pp. 17–52). Singapore: World Scientific.

Rasmussen, P. (2001). Bayesian estimation of change points using the general linear model. *Water Resources Research*, *37*(11), 2723–2731. https://doi.org/10.1029/2001WR000311

Razali, N. M., & Wah, Y. B. (2011). Power comparisons of Shapiro-Wilk, Kolmogorov-Smirnov, Lilliefors and Anserson-Darling tests. *Journal of Statistical Modelling and Analytics*, *2*(1), 21–33.

Read, L. K., & Vogel, R. M. (2015). Reliability, return periods, and risk under nonstationarity. *Water Resources Research*, *51*, 6381–6398. https://doi.org/10.1002/2015WR017089

Rigby, R. A., & Stasinopoulos, D. M. (2005). Generalized additive models for location, scale and shape. *Applied Statistics*, *54*(3), 507–554. https://doi.org/10.1111/j.1467-9876.2005.00510.x

Rippey, B. R. (2015). The U.S. drought of 2012. *Weather and Climate Extremes*, *10*, 57–64. https://doi.org/10.1016/j.wace.2015.10.004

Rootzen, H., & Katz, R. W. (2013). Design life level: Quantifying risk in a changing climate. *Water Resources Research*, *49*, 5964–5972. https://doi.org/10.1002/wrcr.20425

Rosner, A., Vogel, R. M., & Kirshen, P. (2014). A risk-based approach to flood management decisions in a nonstationary world. *Water Resources Research*, *50*, 1928–1942. https://doi.org/10.1002/2013WR014561

Rouge, C., Ge, Y., & Cai, X. (2013). Detecting gradual and abrupt changes in hydrological records. *Advances in Water Resources*, *53*(2012), 33–44. https://doi.org/10.1016/j.advwatres.2012.09.008

Ryu, J., & Hayhoe, K. (2017). Observed and CMIP5 modeled influence of large-scale circulation on summer precipitation and drought in the south-central United States. *Climate Dynamics*, *49*(11-12), 4293–4310. https://doi.org/10.1007/s00382-017-3534-z

Ryu, J.-H., Hayhoe, K., & Kang, S.-L. (2018). Projected changes in summertime circulation patterns imply increased drought risk for the South-Central United States. *Geophysical Research Letters*, *45*, 11,447–11,455. https://doi.org/10.1029/2018GL080593

Salas, J. D., Fu, C., Cancelliere, A., Dustin, D., Bode, D., Pineda, A., & Vincent, E. (2005). Characterizing the severity and risk of drought in the Poudre river, Colorado. *Journal of Water Resources Planning and Management*, *131*(5), 383–393. https://doi.org/10.1061/(ASCE)0733-9496(2005)131:5(383

Salas, J. D., & Obeysekera, J. (2014). Revisiting the concepts of return period and risk for nonstationary hydrologic extreme events. *Journal of Hydrologic Engineering*, *19*(3), 554–568. https://doi.org/10.1061/(ASCE)HE.1943-5584.0000820

Santos, E. G., & Salas, J. D. (1992). Stepwise disaggregation scheme for synthetic hydrology. *Journal of Hydraulic Engineering*, *118*(5), 765–784. https://doi.org/10.1061/(ASCE)0733-9429(1992)118:5(765

Sarhadi, A., Burn, D. H., Ausın, M. C., & Wiper, M. P. (2016). Time-varying nonstationary multivariate risk analysis using a dynamic Bayesian copula. *Water Resources Research*, *52*, 2327–2349. https://doi.org/10.1002/2015WR018525

Schubert, S., Suarez, M., Pegion, P., Koster, R., & Bacmeister, J. (2004b). On the cause of the 1930s Dust Bowl. *Science*, *303*(5665), 1855–1859 . https://doi.org/10.1126/science.1095048

Schubert, S. D., Suarez, M. J., Pegion, P. J., Koster, R. D., & Bacmeister, J. T. (2004a). Causes of long-term drought in the U.S. Great Plains. *Journal of Climate*, *17*(3), 485–503. https://doi.org/10.1175/1520-0442(2004)017<0485:COLDIT>2.0.CO;2

Seager, R., Kushnir, Y., Ting, M., Cane, M., Naik, N., & Miller, J. (2008). Would advance knowledge of 1930s SSTs have allowed prediction of the Dust Bowl drought? *Journal of Climate*, *21*, 3261–3281. https://doi.org/10.1175/2007JCLI2134.1

Serafin, K. A., & Ruggiero, P. (2014). Simulating extreme total water levels using a time-dependent, extreme value approach. *Journal of Geophysical Research: Oceans*, *119*, 6305–6329. https://doi.org/10.1002/2014JC010093

Serinaldi, F. (2011). Distributional modeling and short-term forecasting of electricity prices by generalized additive models for location, scale and shape. *Energy Economics*, *33*(6), 1216–1226. https://doi.org/10.1016/j.eneco.2011.05.001

Serinaldi, F., & Kilsby, C. G. (2012). A modular class of multisite monthly rainfall generators for water resource management and impact studies. *Journal of Hydrology*, *464-465*, 528–540. https://doi.org/10.1016/j.jhydrol.2012.07.043

Serinaldi, F., & Kilsby, C. G. (2014). Simulating daily rainfall fields over large areas for collective risk estimation. *Journal of Hydrology*, *512*, 285–302. https://doi.org/10.1016/j.jhydrol.2014.02.043

Serinaldi, F., & Kilsby, C. G. (2015). Stationarity is undead: Uncertainty dominates the distribution of extremes. *Advances in Water Resources*, *77*, 17–36. https://doi.org/10.1016/j.advwatres.2014.12.013

Sharma, A., Tarboton, D. G., & Lall, U. (1997). Streamflow simulation: A nonparametric approach. *Water Resources Research*, *33*(2), 291–308. https://doi.org/10.1029/96WR02839

She, D., Shao, Q., Xia, J., Taylor, J. A., Zhang, Y., Zhang, L., et al. (2015). Investigating the variation and non-stationarity in precipitation extremes based on the concept of event-based extreme precipitation. *Journal of Hydrology*, *530*, 785–798. https://doi.org/10.1016/j.jhydrol.2015.10.029

Sheffield, J., Camargo, S. J., Fu, R., Hu, Q., Jiang, X., Johnson, N., et al. (2013). North American climate in CMIP5 experiments. Part II: Evaluation of historical simulations of intraseasonal to decadal variability. *Journal of Climate*, *26*(23), 9247–9290. https://doi.org/10.1175/JCLI-D-12-00593.1

Shiau, J. T., & Shen, H. W. (2001). Recurrence analysis of hydrologic droughts of differing severity. *Journal of Water Resources Planning and Management*, *127*(1), 30–40. https://doi.org/10.1061/(ASCE)0733-9496(2001)127:1(30

Singh, D., Swain, D. L., Mankin, J. S., Horton, D. E., Thomas, L. N., Rajaratnam, B., & Diffenbaugh, N. S. (2016). Recent amplification of the North American winter temperature dipole. *Journal of Geophysical Research: Atmospheres*, *121*, 9911–9928. https://doi.org/10.1002/2016JD025116

Sinha, T., Sankarasubramanian, A., & Mazrooei, A. (2014). Decomposition of sources of errors in monthly to seasonal streamflow forecasts in a rainfall–runoff regime. *Journal of Hydrometeorology*, *15*(6), 2470–2483. https://doi.org/10.1175/JHM-D-13-0155.1

Srinivas, V. V., & Srinivasan, K. (2005). Hybrid moving block bootstrap for stochastic simulation of multi-site multi-season streamflows. *Journal of Hydrology*, *302*(1-4), 307–330. https://doi.org/10.1016/j.jhydrol.2004.07.011

Stahl, K., Hisdal, H., Hannaford, J., Tallaksen, L. M., van Lanen, H. A. J., Sauquet, E., et al. (2010). Streamflow trends in Europe: Evidence from a dataset of near natural catchments. *Hydrology and Earth System Sciences*, *14*(12), 2367–2382. https://doi.org/10.5194/hess-14-2367-2010

Stasinopoulos, D. M., & Rigby, R. A. (2007). Generalized additive models for location scale and shape (GAMLSS) in R. *Journal of Statistical Software*, *23*(7), 1–46.

Stedinger, J. R., & Vogel, R. M. (1984). Disaggregation procedures for generating serially correlated flow vectors. *Water Resources Research*, *20*(1), 47–56. https://doi.org/10.1029/WR020i001p00047

Steinschneider, S., & Brown, C. (2013). A semiparametric multivariate, multisite weather generator with low-frequency variability for use in climate risk assessments. *Water Resources Research*, *49*, 7205–7220. https://doi.org/10.1002/wrcr.20528

Steinschneider, S., & Lall, U. (2015). A hierarchical Bayesian regional model for nonstationary precipitation extremes in Northern California conditioned on tropical moisture exports. *Water Resources Research*, *51*, 1472–1492. https://doi.org/10.1002/2014WR016664

Sun, X., Lall, U., Merz, B., & Dung, N. V. (2015). Hierarchical Bayesian clustering for nonstationary flood frequency analysis: Application to trends of annual maximum flow in Germany. *Water Resources Research*, *51*, 6586–6601. https://doi.org/10.1002/2015WR017117

Tan, X., & Gan, T. Y. (2015). Nonstationary analysis of annual maximum streamflow of Canada. *Journal of Climate*, *28*(5), 1788–1805. https://doi.org/10.1175/JCLI-D-14-00538.1

Tarboton, D. G., Sharma, A., & Lall, U. (1998). Disaggregation procedures for stochastic hydrology based on nonparametric density estimation. *Water Resources Research*, *34*(1), 107–119. https://doi.org/10.1029/97WR02429

Tootle, G. A., Piechota, T. C., & Singh, A. (2005). Coupled oceanic–atmospheric variability and U.S. streamflow. *Water Resources Research*, *41*, W12408. https://doi.org/10.1029/2005WR004381

Towler, E., Rajagopalan, B., Gilleland, E., Summers, R. S., Yates, D., & Katz, R. W. (2010). Modeling hydrologic and water quality extremes in a changing climate: A statistical approach based on extreme value theory. *Water Resources Research*, *46*, W11504. https://doi.org/10.1029/2009WR008876

Trenberth, K. E., Fasullo, J. T., & Smith, L. (2005). Trends and variability in column-integrated atmospheric water vapor. *Climate Dynamics*, *24*(7-8), 741–758. https://doi.org/10.1007/s00382-005-0017-4

Tye, M. R., Blenkinsop, S., Fowler, H. J., Stephenson, D. B., & Kilsby, C. G. (2016). Simulating multimodal seasonality in extreme daily precipitation occurrence. *Journal of Hydrology*, *537*, 117–129. https://doi.org/10.1016/j.jhydrol.2016.03.038

Valencia, D., & Schakke, J. C. (1973). Disaggregation processes in stochastic hydrology. *Water Resources Research*, *9*(3), 580–585. https://doi.org/10.1029/WR009i003p00580

Verdin, A., Rajagopalan, B., Kleiber, W., Podesta, G., & Bert, F. (2015). A conditionalstochastic weather generator for seasonal to multi-decadal simulations. *Journal of Hydrology*, *556*, 835–846. https://doi.org/10.1016/j.jhydrol.2015.12.036

Villarini, G., & Serinaldi, F. (2012). Development of statistical models for at-site probabilistic seasonal rainfall forecast. *International Journal of Climatology*, *32*, 2,197–2,212. https://doi.org/10.1002/joc.3393

Villarini, G., Serinaldi, F., Smith, J. A., & Krajewski, W. F. (2009). On the stationarity of annual flood peaks in the continental United States during the 20th century. *Water Resources Research*, *45*, W08417. https://doi.org/10.1029/2008WR007645

Villarini, G., Smith, J. A., & Napolitano, F. (2010). Nonstationary modeling of a long record of rainfall and temperature over Rome. *Advances in Water Resources*, *33*(10), 1256–1267. https://doi.org/10.1016/j.advwatres.2010.03.013

Villarini, G., Smith, J. A., Ntelekos, A. A., & Schwarz, U. (2011). Annual maximum and peaks-over-threshold analyses of daily rainfall accumulations for Austria. *Journal of Geophysical Research*, *116*, D05103. https://doi.org/10.1029/2010JD015038

Villarini, G., Smith, J. A., Serinaldi, F., Bales, J., Bates, P. D., & Krajewski, W. F. (2009). Flood frequency analysis for nonstationary annual peak records in an urban drainage basin. *Advances in Water Resources*, *32*(8), 1255–1266. https://doi.org/10.1016/j.advwatres.2009.05.003

Vittal, H., Karmakar, S., & Ghosh, S. (2013). Diametric changes in trends and patterns of extreme rainfall over India from pre-1950 to post-1950. *Geophysical Research Letters*, *40*, 3253–3258. https://doi.org/10.1002/grl.50631

Vogel, R. M., Yaindl, C., & Walter, M. (2011). Nonstationarity: Flood magnification and recurrence reduction factors in the United States. *Journal of the American Water Resources Association*, *47*(3), 464–474. https://doi.org/10.1111/j.1752-1688.2011.00541.x

Volpi, E., Fiori, A., Grimaldi, S., Lombardo, L., & Koutsoyiannis, D. (2015). One hundred years of return period: Strengths and limitations. *Water Resources Research*, *51*, 8570–8585. https://doi.org/10.1002/2015WR017820

Wang, H., Brill, E. D., Ranjithan, R. J., & Sankarasubramanian, A. (2015). A framework for incorporating ecological releases in single reservoir operation. *Advances in Water Resources*, *78*, 9–21. https://doi.org/10.1016/j.advwatres.2015.01.006

Wang, S.-Y., Hipps, L., Gillies, R. R., & Yoon, J. H. (2014). Probable causes of the abnormal ridge accompanying the 2013–2014 California drought: ENSO precursor and anthropogenic warming footprint. *Geophysical Research Letters*, *41*, 3220–3226. https://doi.org/10.1002/2014GL059748

Wilhite, D. A., Hayes, M. J., Knutson, C., & Smith, K. H. (2000). Planning for drought: Moving from crisis to risk management. *Journal of the American Water Resources Association*, *36*(4), 697–710. https://doi.org/10.1111/j.1752-1688.2000.tb04299.x

Wilks, D. S. (1999). Interannual variability and extreme-value characteristics of several stochastic daily precipitation models. *Agricultural and Forest Meteorology*, *93*(3), 153–169. https://doi.org/10.1016/S0168-1923(98)00125-7

Wilks, D. S. (2006). On "field significance" and the false discovery rate. *Journal of Applied Meteorology and Climatology*, *45*(9), 1181–1189. https://doi.org/10.1175/JAM2404.1

Wong, H., Hu, B. Q., Ip, W. C., & Xia, J. (2006). Change-point analysis of hydrological time series using grey relational method. *Journal of Hydrology*, *324*(1-4), 323–338. https://doi.org/10.1016/j.jhydrol.2005.10.007

World Meteorological Organization. (2006). Drought monitoring and early warning: Concepts, progress and future challenges. WMO Report 1006, World Meteorol. Org.

Xie, H., Li, D., & Xiong, L. (2014). Exploring the ability of the Pettitt method for detecting change point by Monte Carlo simulation. *Stochastic Environmental Research and Risk Assessment*, *28*(7), 1643–1655. https://doi.org/10.1007/s00477-013-0814-y

Xiong, B., Xiong, L., Chen, J., Xu, C.-Y., & Li, L. (2018). Multiple causes of nonstationarity in the Weihe annual low-flow series. *Hydrology and Earth System Sciences*, *22*(2), 1525–1542. https://doi.org/10.5194/hess-22-1525-2018

Xiong, L., Jiang, C., Xu, C.-Y., Yu, K. X., & Guo, S. (2015). A framework of change point detection for multivariate hydrological series. *Water Resources Research*, *51*, 8198–8217. https://doi.org/10.1002/2015WR017677

Yoon, J. H., Wang, S.-Y., Gillies, R. G., Kravitz, B., Hipps, L., & Rasch, P. J. (2015). Increasing water cycle extremes in California in relation to ENSO cycle under global warming. *Nature Communications*, *6*(1), 8657. https://doi.org/10.1038/ncomms9657

Yue, S., Pilon, P., & Cavadias, G. (2002). Power of the Mann–Kendall and Sperman's rho tests for detecting monotonic trends in hydrological series. *Journal of Hydrology*, *259*(1-4), 254–271. https://doi.org/10.1016/S0022-1694(01)00594-7

Zhang, Q., Gu, X., Singh, V. P., Xiao, M., & Chen, X. (2015). Evaluation of flood frequency under non-stationarity resulting from climate indices and reservoir indices in the East River Basin, China. *Journal of Hydrology*, *527*, 565–575. https://doi.org/10.1016/j.jhydrol.2015.05.029

Zhang, Q., Gu, X., Singh, V. P., Xiao, M., & Xu, C. Y. (2014). Stationarity of annual flood peaks during 1951–2010 in the Pearl River Basin, China. *Journal of Hydrology*, *519*, 3263–3274. https://doi.org/10.1016/j.jhydrol.2014.10.028